Clinical Investigations

Impact of Systolic Dysfunction in Genotyped Hypertrophic Cardiomyopathy

Address for correspondence:
Noboru Fujino, MD
Division of Cardiovascular Medicine
Kanazawa University Graduate
School of Medical Science
Takara-machi 13-1
Kanazawa-City,
Ishikawa-Prefecture, Japan
nfujino@mhs.mp.kanazawa-u.ac.jp

Noboru Fujino, MD; Tetsuo Konno, MD; Kenshi Hayashi, MD; Akihiko Hodatsu, MD; Takashi Fujita, MD; Toyonobu Tsuda, MD; Yoji Nagata MD; Masa-aki Kawashiri, MD; Hidekazu Ino, MD; Masakazu Yamagishi, MD
Division of Cardiovascular Medicine, Kanazawa University Graduate School of Medical Science, Kanazawa-City, Japan

ABSTRACT

Background: Hypertrophic cardiomyopathy (HCM) is a disease of the sarcomere, and approximately 5% of cases of HCM show systolic dysfunction with poor prognosis. Few data exist regarding the systolic dysfunction in a large population of genotyped HCM subjects.

Hypothesis: The aim of this study was to assess the systolic dysfunction and prognosis in sarcomere gene mutation carriers.

Methods: The study included 157 sarcomere gene mutation carriers from 69 unrelated HCM families (87 males; mean age, 46.5 ± 20.5 years). After exclusions for systolic dysfunction at baseline, 107 subjects underwent serial echocardiograms.

Results: At a mean follow-up of 7.0 years, 12 subjects experienced systolic dysfunction. In multivariate Cox analysis, systolic dysfunction was related to age and ejection fraction at initial evaluation ($P < 0.001$ and $P = 0.020$, respectively), and was associated with the absence of mutations in the cardiac myosin-binding protein C gene (*MYBPC3*) ($P = 0.042$). When the subjects were divided into *MYBPC3* and non-*MYBPC3* mutation carriers, and time from birth to development of systolic dysfunction was compared, the rate of systolic dysfunction was higher in the non-*MYBPC3* group than in *MYBPC3* group (Kaplan-Meier, log-rank test, $P = 0.010$). After the onset of systolic dysfunction, 11 of 12 subjects died during a mean follow-up of 8.3 years.

Conclusions: Non-*MYBPC3* mutation carriers developed left ventricular systolic dysfunction more frequently than *MYBPC3* mutation carriers, and the majority of sarcomere gene mutation carriers with systolic dysfunction had fatal outcomes during follow-up. This suggests that subjects with mutations in sarcomeric genes require careful management for systolic dysfunction.

Introduction

Hypertrophic cardiomyopathy (HCM) is a primary disorder of the myocardium that causes distinctive anatomic and histologic features,[1] and it is the most frequent cause of sudden cardiac death in young athletes.[2] Epidemiologic data indicate that 2 in 1000 young adults have unexplained hypertrophy.[3] Mutations in genes that encode sarcomere proteins including cardiac myosin-binding protein C gene (*MYBPC3*), cardiac troponin T gene (*TNNT2*), cardiac troponin I gene (*TNNI3*), and cardiac β-myosin heavy chain gene (*MYH7*) are well-established causes of the disease.[1,4] Studies in populations with familial HCM often reported that mutations in sarcomere proteins could be detected in around 50% of study subjects.[4–6] Left ventricular systolic dysfunction has been regarded as a relatively common disease complication of HCM.[7–10] However, the characterization of left ventricular systolic dysfunction has been hindered by the small number of subjects with the disease (single cases or small groups of subjects).[11–13] We have reported that subjects with HCM caused by mutations in *TNNT2* and *TNNI3* start to develop left ventricular systolic dysfunction at around 40 years of age.[14–17] In addition, we and others have reported that subjects with HCM caused by mutations in *MYBPC3* also progress to left ventricular systolic dysfunction,[18,19] although the clinical features of HCM associated with mutations in *MYBPC3* have late onset and a favorable clinical course.[20] These data may provide useful information on genetic counseling strategies of affected subjects with sarcomere gene mutations. However, these previous studies have been based largely on HCM subjects with a single gene mutation.[14–19]

The primary aim of the present study was to compare the clinical course of left ventricular systolic dysfunction

This work was supported in part by a Grant-in-Aid for Scientific Research, the Ministry of Education, Culture, Sports, Science, and Technology (KAKENHI 16790414, 19590807, 22590808, Tokyo, Japan), and the Research Grant for Cardiovascular Diseases (20C-4) from the Ministry of Health, Labour, and Welfare (Tokyo, Japan).
The authors have no other funding, financial relationships, or conflicts of interest to disclose.

Clin. Cardiol. 36, 3, 160–165 (2013)
Published online in Wiley Online Library (wileyonlinelibrary.com)
DOI:10.1002/clc.22082

Received: September 4, 2012
Accepted with revision: October 31, 2012

in subjects with HCM in a relatively large population with mutations in various sarcomeric genes. The secondary aim was to assess the prognosis of the HCM subjects who developed left ventricular systolic dysfunction.

Methods

This study included 69 unrelated probands with HCM exhibiting disease-causing mutations in genes such as *MYBPC3*, *TNNT2*, *TNNI3*, and *MYH7*. In addition, their family members were evaluated clinically and genetically, and 88 carriers with the same etiological sarcomere gene mutation as each proband were identified. Thus, a total 157 genetically affected subjects (87 males; mean age, 46.5 ± 20.5 years) comprised the study population. All subjects were identified at Kanazawa University Hospital or its affiliated hospitals (from primary to tertiary care centers) between 1998 and 2009. The diagnosis of HCM was based on the echocardiographic demonstration of left ventricular hypertrophy (LVH) (maximal left ventricular wall thickness ≥13 mm) in the absence of other cardiac or systemic causes for the left ventricular hypertrophy. These subjects also met the definition and classification proposed by the 1995 World Health Organization/International Society and Federation of Cardiology Task Force.[21] Subjects with systolic dysfunction were also included in this study. To compare the differences in the clinical course between several disease-causing genes, carriers with multiple mutations were not included in this study. Written informed consent was obtained from all subjects or from the parents of minors participating in the study in accordance with the guidelines of the Bioethical Committee on Medical Research, Graduate School of Medical Science, Kanazawa University, Kanazawa, Japan.

DNA was isolated from peripheral white blood cells of all subjects by use of a DNA extractor (ABI 341 Genepure Nucleic Acid Purification System; Applied Biosystems, Carlsbad, CA). In vitro amplification of genomic DNA was performed via polymerase chain reaction (PCR). Oligonucleotide primers were used to amplify all exons and exon-intron boundaries of 4 sarcomere genes, namely *MYBPC3*, *TNNT2*, *TNNI3*, and *MYH7* using standard protocols as previously described.[14–18] Single-strand conformational polymorphism analysis of amplified DNA was then performed as previously described,[14–18] with a slight modification. We also screened for mutations in sarcomere genes using high-resolution melt analysis as previously described.[22] For abnormal single-strand conformational polymorphism patterns or abnormal melt profiles, the nucleotide sequences of the cloned PCR products were determined on both strands (bidirectional sequencing) by the dye terminator cycle sequencing method using an automated fluorescent sequencer (ABI PRISM 310 Genetic Analyzer; Applied Biosystems). The sequence variation was confirmed by restriction enzyme digestion. Samples from 400 chromosomes of 200 ethnicity-matched normal individuals were also analyzed.

Standard transthoracic M-mode and 2-dimensional echocardiographic studies were performed to identify and quantify the morphological features of the left atrium and left ventricle. The left atrial dimension was measured at end-systole. Maximal wall thickness (MWT) of the left ventricle was defined as the greatest thickness in any single segment. Left ventricular end-diastolic dimension (LVDd), left ventricular end-systolic dimension (LVDs), interventricular septal thicknesses (IVST), and posterior wall thickness (PWT) were measured at the level of the tips of the mitral valve leaflets. Ejection fraction (EF) was calculated by Teicholz's method and by modified Simpson's method when left ventricular dilatation or regional decrease of left ventricular wall motion occurred. Systolic dysfunction was defined as EF <50% according to a previous report.[23] The echocardiographic parameters and the course of development of systolic dysfunction were compared among the genotyped HCM subjects. Differences between values measured at baseline and follow-up were analyzed by the Student paired *t* test. Differences between groups were analyzed by the Student unpaired *t* test. Categorical variables were compared by the χ^2 test for independent variables. A multivariate Cox analysis was performed to find predictor factors of systolic dysfunction. The age that subjects developed systolic dysfunction for the first time was estimated according to the Kaplan-Meier method, and comparison of the 2 groups was performed by means of the log-rank test. A P value <0.05 was considered statistically significant in all analyses. Statistical analyses were carried out with the computer software SPSS version 17.0 (IBM SPSS, Armonk, NY).

Results

The clinical and genetic characteristics of the study population are presented in Table 1; 26 different mutations were identified in 157 subjects. Left ventricular outflow tract obstruction (pressure gradient at rest >30 mm Hg) was detected only in 4 subjects (hypertrophic obstructive cardiomyopathy), and none of them underwent percutaneous septal ablation. Most of these mutations have been identified and described elsewhere.[14–19,24–27] Three nonsense mutations, p.Gln541ter, p.Tyr816ter, and p.Gln827ter in *MYBPC3* and 3 missense mutations, p.Ala200Thr, p.Ala321Val, and p.Ser866Pro in *MYH7* were novel and presumed to be pathogenic by standard criteria of the absence of the mutation in large numbers of normal controls, alteration of evolutionarily conserved residues, and/or predicted impact on protein structure. Two missense mutations p.Val85Leu in *TNNT2* and the missense mutation p.Met822Leu in *MYH7* were due to alteration in the nucleotide sequences, GTG to TTG, ATG to CTG, respectively; this the first report of these nucleotide alterations in these genes.

At the initial evaluation, 9 subjects showed systolic dysfunction. Of the 9 subjects, 3 were *MYBPC3* mutation carriers (2 of p.Arg820Gln from 2 families and 1 of p.Gln998Glu), 2 were *TNNT2* mutation carriers (both p.Arg92Trp from 1 family), 2 were *TNNI3* mutation carriers (both p.Lys183del from 2 families), and 2 were *MYH7* mutation carriers (1 of p.Gly733Glu and 1 of p.Met822Leu). As for the frequencies of subjects with systolic dysfunction, 5.4% (3/56) were *MYBPC3* mutation carriers, 8.7% (2/23) were *TNNT2* mutation carriers, 3.6% (2/56) were *TNNI3* mutation carriers, and 9.1% (2/22) were *MYH7* mutation carriers. There were no differences among the carriers

Published online in Wiley Online Library (wileyonlinelibrary.com)
DOI:10.1002/clc.22082

Table 1. Clinical and Genetic Characteristics of the Study Population

No.	157
Age (y)	46.5 ± 20.5
Male (%)	87 (55.4)
Echocardiography	
LAD (mm)	37.6 ± 7.5
IVST (mm)	14.7 ± 5.4
PWT (mm)	10.5 ± 2.3
MWT (mm)	15.3 ± 5.6
LVDd (mm)	44.5 ± 6.3
LVDs (mm)	28.0 ± 7.0
EF (%)	67.1 ± 10.9
HOCM	4 (2.5%)
Disease-causing gene (%)	
MYBPC3	56 (35.7)
TNNT2	23 (14.6)
TNNI3	56 (35.7)
MYH7	22 (14.0)
Medications (%)	
Calcium channel blocker	27 (17.2)
β-Blocker	24 (15.3)
ACE-I or ARB blocker	29 (18.5)

Abbreviations: ACE-I, angiotensin-converting enzyme-inhibitor; ARB, angiotensin receptor blocker; EF, ejection fraction; HOCM, hypertrophic obstructive cardiomyopathy; IVST, interventricular septal thickness; LAD, left atrial dimension; LVDd, left ventricular end-diastolic dimension; LVDs, left ventricular end-systolic dimension; MWT, maximal wall thickness; *MYBPC3*, cardiac myosin-binding protein C gene; *MYH7*, cardiac β-myosin heavy chain gene; PWT, posterior wall thickness; *TNNI3*, cardiac troponin I gene; *TNNT2*, cardiac troponin T gene. Values are mean ± SD unless otherwise shown.

of the 4 genes with respect to the frequency of systolic dysfunction ($P = 0.72$). To study the clinical course of the development of systolic dysfunction, 9 subjects who had systolic dysfunction at the initial evaluation were excluded, and 107 of the 157 subjects underwent serial echocardiography at least a month apart. The data from 107 subjects (54 males; mean age, 44.7 ± 20.9 years; mean follow-up, 7.0 ± 4.9 years) were analyzed. During the mean follow-up period of 7 years, 12 subjects out of 107 experienced systolic dysfunction (1.60 cases per 100 person-years). In multivariate Cox analysis, systolic dysfunction was closely related to the age and ejection fraction at initial evaluation ($P < 0.001$ and $P = 0.020$, respectively), and was closely related to the absence of mutation in *MYBPC3* as a disease-causing gene ($P = 0.042$). Therefore, we divided the 107 subjects into 2 groups, those with *MYBPC3* mutations and those with other sarcomere gene mutations (non-*MYBPC3*), and compared the age to the development of systolic dysfunction.

Table 2. Serial Changes of Echocardiographic Parameters During Follow-up

	Baseline	*P* Value	Follow-up	*P* Value
Cases				
MYBPC3	36			
Non-*MYBPC3*	71			
Male (%)				
MYBPC3	24 (66.7)	0.017		
Non-*MYBPC3*	30 (42.3)			
Age, y				
MYBPC3	50.1 ± 19.9	0.055		
Non-*MYBPC3*	41.9 ± 21.0			
HOCM (%)				
MYBPC3	2 (5.6)	0.480		
Non-*MYBPC3*	2 (2.8)			
Medications (%)				
Calcium channel blocker				
MYBPC3	8 (22.2)	0.721		
Non-*MYBPC3*	18 (25.4)			
β-Blocker				
MYBPC3	5 (13.9)	0.287		
Non-*MYBPC3*	16 (22.5)			
ACE-I or ARB				
MYBPC3	7 (19.4)	0.598		
Non-*MYBPC3*	17 (23.9)			
IVST				
MYBPC3	15.8 ± 5.6	0.565	17.2 ± 6.0	0.118
Non-*MYBPC3*	15.1 ± 5.6		15.4 ± 5.5	
PWT				
MYBPC3	11.1 ± 2.3	0.178	10.4 ± 1.8	0.529
Non-*MYBPC3*	10.4 ± 2.6		10.2 ± 2.5	
MWT				
MYBPC3	16.6 ± 5.9	0.456	17.5 ± 6.0	0.194
Non-*MYBPC3*	15.7 ± 5.8		15.9 ± 5.9	
LVDd				
MYBPC3	43.8 ± 4.9	0.754	44.9 ± 5.8	0.717
Non-*MYBPC3*	43.5 ± 5.5		44.4 ± 7.0	

There were 36 subjects in *MYBPC3* and 71 subjects in non-*MYBPC3* groups. At the time of initial evaluation,

Table 2. *Continued*

	Baseline	*P* Value	Follow-up	*P* Value
LVDs				
MYBPC3	26.5 ± 3.8	0.829	27.7 ± 5.5	0.344
Non-*MYBPC3*	26.7 ± 5.1		29.1 ± 7.9[a]	

Abbreviations: ACE-I, angiotensin-converting enzyme-inhibitor; ARB, angiotensin receptor blocker; HOCM, hypertrophic obstructive cardiomyopathy; IVST, interventricular septal thickness; LVDd, left ventricular end-diastolic dimension; LVDs, left ventricular end-systolic dimension; MWT, maximal wall thickness; PWT, posterior wall thickness. Values are mean ± standard deviation unless otherwise shown. *P* values concern the comparison of the values at baseline and follow-up between *MYBPC3* and non-*MYBPC3* (12 of *TNNT2*, 46 of *TNNI3*, and 13 of *MYH7*). [a]P < 0.05 compared with baseline within group by paired *t* test.

no significant differences were found between *MYBPC3* and non-*MYBPC3* groups, respectively, for the following variables: IVST, PWT, MWT, LVDd, and LVDs (Table 2). There was no significant difference in EF between the 2 groups at baseline. However, the percent decrease in EF was significantly greater in the non-*MYBPC3* group between baseline and last evaluation or the time of development of systolic dysfunction (69.0 ± 8.4% vs 63.7 ± 13.0%; $P < 0.001$) (Figure 1), whereas there was no significant change in the *MYBPC3* group in this time interval. Furthermore, Kaplan-Meier analysis comparing the age at which systolic dysfunction developed showed a significant difference between *MYBPC3* and non-*MYBPC3* groups (log-rank test, $P = 0.010$) (Figure 2). In the *MYBPC3* group, 1 subject out of 36 subjects developed to systolic dysfunction at the age of 71 in 6.3 years (0.44 cases per 100 person-years). On the other hand, in the non-*MYBPC3* group, 11 subjects out of 71 subjects developed to systolic dysfunction in 7.3 years (2.12 cases per 100 person-years, $P = 0.093$).

Next, we investigated the prognosis of the 12 subjects who developed systolic dysfunction (Table 3). Systolic dysfunction had a wide range of age for onset (ie, 41 to 74 years; mean, 58.9 ± 11.9 years). Three subjects (25.0%) were 41 to 50 years old, 4 subjects (33.3%) were 51 to 60 years old, 1 subject (8.3 %) had onset age of 62, and 4 subjects (33.3 %) were over 70 years old. Four subjects (33.3%) were male, and the mean age at death or the most recent evaluation was 67.3 ± 11.5 years. All 12 subjects were admitted to hospital for heart failure, and 11 out of 12 subjects (91.7%) died within the follow-up period (8.3 ± 4.0 years). Four out of 11 subjects (36.4%) died of refractory heart failure, 4 subjects (36.4%) died suddenly from causes related to heart failure, 2 subjects (18.2%) died of interstitial pneumonia after heart failure, and 1 subject (9.1%) died of cerebral infarction with atrial fibrillation with use of an appropriate dose of warfarin.

Discussion

In this longitudinal study, 107 of the 157 genotyped HCM subjects underwent serial echocardiography, and during the mean follow-up period of 7 years, 12 subjects out of 107 experienced systolic dysfunction (1.60 cases per 100 person-years). The major finding was, that in a relatively large population of genotyped HCM subjects, EF decreased significantly in the non-*MYBPC3* group (69.0 ± 8.0% to 63.7 ± 13.0%, $P < 0.001$) (Figure 1), and freedom from systolic dysfunction was lower in subjects in the non-*MYBPC3* group than those in *MYBPC3* group (Kaplan-Meier, log-rank test, $P = 0.010$) (Figure 2).

The clinical features of HCM are particularly heterogeneous.[7,8] A patient subset characterized by clinical progression of left ventricular systolic dysfunction has been described.[9–13] Most of the prior literature about systolic dysfunction is, however, limited to isolated or small groups of subjects.[9–13] Recently, Harris et al reported on a cohort of HCM subjects with systolic dysfunction in a multicenter study that included the largest group of subjects with systolic dysfunction reported to date.[23] In that study, incidence of systolic dysfunction was 1.12 cases per 100 person-years. In our study, incidence of systolic dysfunction was 12 cases per 749 person-years of follow-up (1.60 cases per 100 person-years); the rates in these 2 studies were similar, which suggests that the cohort of 157 genotyped HCM subjects in this study was comparable to the cohort of 1259 study subjects in the former study in terms of systolic dysfunction.

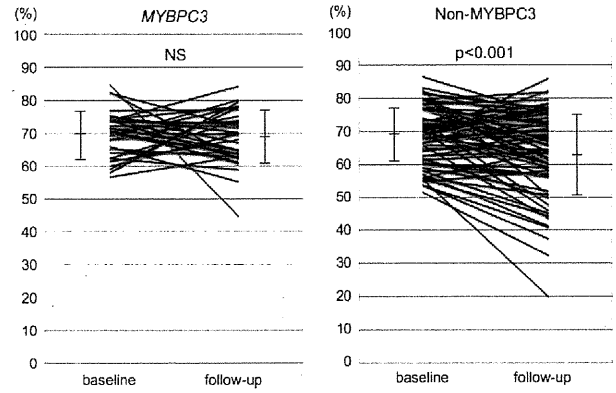

Figure 1. The percent decrease in ejection fraction in *MYBPC3* and non-*MYBPC3* groups. *MYBPC3*, myosin-binding protein C gene; NS, not significant.

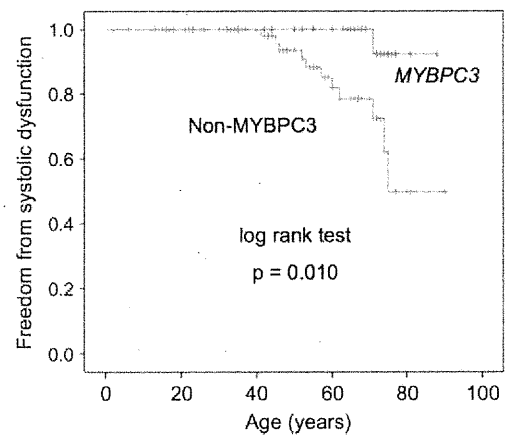

Figure 2. Kaplan-Meier analysis comparing the age at which systolic dysfunction developed in subjects in the myosin-binding protein C (*MYBPC3*) gene and non-*MYBPC3* groups.

Published online in Wiley Online Library (wileyonlinelibrary.com)
DOI:10.1002/clc.22082

Recent advances in molecular genetics have demonstrated that HCM can be considered as a disease of the sarcomere. Some studies have investigated the relationship between specific sarcomere gene mutation and systolic dysfunction; however, these were limited to subjects with mutations in a single gene only.[14–19] In the multicenter cohort of over 1200 HCM subjects,[23] 44 subjects demonstrated systolic dysfunction, and 3 probands were genotyped to HCM-causing sarcomere protein mutations: p.Gly716Arg in *MYH7* in 2 and G-791 in *MYBPC3* in 1. This number of subjects (6.8%, 3 of 44) is very limited. On the other hand, we studied a relatively large population of HCM subjects with several sarcomere gene mutations and analyzed the relationship between disease-causing genes and systolic dysfunction.

We found that freedom from systolic dysfunction was lower in subjects in the non-*MYBPC3* group than those in *MYBPC3* group in this longitudinal study (Kaplan-Meier, log-rank test, $P = 0.010$) (Figure 2). This could be explained by several findings in the recent study. Sakata et al investigated left ventricular function reserve in HCM patients with and without mutations in cardiac troponin genes (*TNNT2* and *TNNI3*) before transition to systolic dysfunction.[28] Interestingly, the group of subjects with troponin gene mutations showed a significant increase in left ventricular end-systolic volume during an exercise test. This suggests that subjects with troponin gene mutations display exercise-induced left ventricular systolic dysfunction more frequently than HCM subjects without troponin gene mutations. The authors speculated that the mechanism of the systolic dysfunction was myocardial ischemia due to lumen narrowing of intramural coronary arteries. It was reported that the use of calcium channel blockers in advance of established clinical disease could prevent HCM caused by sarcomere protein gene mutations in a mouse model,[29] therefore the use of calcium channel blockers to ameliorate ischemia in advance of established systolic dysfunction may be useful to prevent the progression to systolic dysfunction in HCM.

Next, we investigated the prognosis of the 12 subjects who developed systolic dysfunction during follow-up (Table 3). At the time of presentation of systolic dysfunction, the mean age of the 12 subjects was 58.9 years (range, 41–74 years) and 67.3 years (range, 51–84 years) at death or the most recent evaluation. All of the 12 subjects were admitted to the hospital for heart failure, and 11 out of 12 subjects (91.7%) died within the follow-up period, which means the prognosis of genotyped subjects with HCM demonstrating systolic dysfunction is poor. The present study demonstrated that HCM subjects with mutations in sarcomere-related genes other than *MYBPC3* develop left ventricular systolic dysfunction more frequently than those with *MYBPC3* mutations, and most of those who developed systolic dysfunction died within mean period of 8.3 years. These observations may provide important prognostic information in the clinical practice of HCM, which suggests that subjects with mutations in sarcomeric genes require careful management for systolic dysfunction from the point of view of prognosis.

There remain several limitations of the present study. First, in recent studies, multiple gene mutations have been reported, which may further contribute to the disease heterogeneity.[30–35] We did not include carriers with multiple mutations in this study to compare the differences in the clinical course between multiple disease-causing genes; however, we should also assess the influence of multiple mutations on HCM phenotype as the next step. Second, heart transplantation should have been considered for many subjects who showed systolic dysfunction in our study; however, heart transplantation is not common in Japan. It

Table 3. Clinical Data From 12 Subjects Who Showed Systolic Dysfunction During Follow-up

No.	Gene	Gender	A, y	Last Evaluation	B, y	A to B, y	Etiology of Death
1	*MYBPC3*	Male	71	Death	76	5	Interstitial pneumonia after heart failure
2	*MYH7*	Male	74	Death	78	4	Sudden death during heart failure
3	*TNNT2*	Female	60	Death	69	9	Refractory heart failure
4	*TNNT2*	Female	53	Death	62	9	Refractory heart failure
5	*TNNI3*	Female	46	Death	52	6	Sudden death during chronic heart failure
6	*TNNI3*	Female	52	Death	59	7	Sudden death during heart failure
7	*TNNI3*	Female	45	Death	51	6	Refractory heart failure
8	*TNNI3*	Female	57	Death	74	17	Cerebral infarction with atrial fibrillation
9	*TNNI3*	Female	71	Death	84	13	Refractory heart failure
10	*TNNI3*	Male	62	Death	70	8	Interstitial pneumonia after hear failure
11	*TNNI3*	Male	75	Death	79	4	Sudden death during chronic heart failure
12	*TNNI3*	Female	41	Alive	53	12	Not available
			58.9 ± 11.9		67.3 ± 11.5	8.3 ± 4.0	

Abbreviations: A, age at systolic dysfunction; A to B, interval from A to B; B, age at death or last evaluation.

Published online in Wiley Online Library (wileyonlinelibrary.com)
DOI:10.1002/clc.22082

appears that without the option of heart transplantation, the natural course of systolic dysfunction related to sarcomere genes mutations often follows an adverse course with fatal outcome. Last, 46 out of the 71 subjects in the non-*MYBPC3* group were *TNNI3* mutation carriers (Table 2), which might reflect a founder effect. However, we also included subjects with mutations in *MYBPC3* that were reported to be associated with systolic dysfunction.[18,19]

Conclusion

Non-*MYBPC3* mutation carriers developed left ventricular systolic dysfunction more frequently than *MYBPC3* mutation carriers, and the majority of sarcomere gene mutation carriers with systolic dysfunction had fatal outcomes during follow-up. This suggests that subjects with mutations in sarcomeric genes require careful management for systolic dysfunction.

References

1. Seidman JG, Seidman C. The genetic basis for cardiomyopathy: from mutation identification to mechanistic paradigms. *Cell.* 2001;104:557–567.
2. Maron BJ, Shirani J, Poliac LC, et al. Sudden death in young competitive athletes. Clinical, demographic, and pathological profiles. *JAMA.* 1996;276:199–204.
3. Maron BJ, Gardin JM, Flack JM, et al. Prevalence of hypertrophic cardiomyopathy in a general population of young adults. Echocardiographic analysis of 4111 subjects in the CARDIA Study. Coronary Artery Risk Development in (Young) Adults. *Circulation.* 1995;92:785–789.
4. Arad M, Seidman JG, Seidman CE. Phenotypic diversity in hypertrophic cardiomyopathy. *Hum Mol Genet.* 2002;11:2499–2506.
5. Kimura A, Harada H, Park JE, et al. Mutations in the cardiac troponin I gene associated with hypertrophic cardiomyopathy. *Nat Genet.* 1997;16:379–382.
6. Spirito P, Seidman CE, McKenna WJ, et al. The management of hypertrophic cardiomyopathy. *N Engl J Med.* 1997;336:775–785.
7. Maron BJ. Hypertrophic cardiomyopathy: a systematic review. *JAMA.* 2002;287:1308–1320.
8. Maron BJ, McKenna WJ, Danielson GK, et al. American College of Cardiology/European Society of Cardiology clinical expert consensus document on hypertrophic cardiomyopathy. *J Am Coll Cardiol.* 2003;42:1687–1713.
9. Maron BJ, Spirito P. Implications of left ventricular remodeling in hypertrophic cardiomyopathy. *Am J Cardiol.* 1998;81:1339–1344.
10. Spirito P, Maron BJ, Bonow RO, et al. Occurrence and significance of progressive left ventricular wall thinning and relative cavity dilatation in patients with hypertrophic cardiomyopathy. *Am J Cardiol.* 1987;60:123–129.
11. Maron BJ, Epstein SE, Roberts WC. Hypertrophic cardiomyopathy and transmural myocardial infarction without significant atherosclerosis of the extramural coronary arteries. *Am J Cardiol.* 1979;43:1086–1102.
12. Shirani J, Maron BJ, Cannon RO, et al. Clinicopathologic features of hypertrophic cardiomyopathy managed by cardiac transplantation. *Am J Cardiol.* 1993;72:434–440.
13. Hecht GM, Klues HG, Roberts WC, et al. Coexistence of sudden cardiac death and end-stage heart failure in familial hypertrophic cardiomyopathy. *J Am Coll Cardiol.* 1993;22:489–497.
14. Kokado H, Shimizu M, Yoshio H, et al. Clinical features of hypertrophic cardiomyopathy caused by a Lys183 deletion mutation in the cardiac troponin I gene. *Circulation.* 2000;102:663–669.
15. Fujino N, Shimizu M, Ino H, et al. Cardiac troponin T Arg92Trp mutation and progression from hypertrophic to dilated cardiomyopathy. *Clin Cardiol.* 2001;24:397–402.
16. Fujino N, Shimizu M, Ino H, et al. A novel mutation Lys273Glu in the cardiac troponin T gene shows high degree of penetrance and transition from hypertrophic to dilated cardiomyopathy. *Am J Cardiol.* 2002;89:29–33.
17. Shimizu M, Ino H, Okeie K, et al. Septal wall thinning and systolic dysfunction in patients with hypertrophic cardiomyopathy caused by a cardiac troponin I gene mutation. *Am Heart J.* 2002;143:690–695.
18. Konno T, Shimizu M, Ino H, et al. A novel missense mutation in the myosin binding protein-C gene is responsible for hypertrophic cardiomyopathy with left ventricular dysfunction and dilation in elderly patients. *J Am Coll Cardiol.* 2003;41:781–786.
19. Kubo T, Kitaoka H, Okawa M, et al. Lifelong left ventricular remodeling of hypertrophic cardiomyopathy caused by a founder frameshift deletion mutation in the cardiac myosin-binding protein C gene among Japanese. *J Am Coll Cardiol.* 2005;46:1737–1743.
20. Niimura H, Bachinski LL, Sangwatanaroj S, et al. Mutations in the gene for cardiac myosin-binding protein C and late-onset familial hypertrophic cardiomyopathy. *N Engl J Med.* 1998;338:1248–1257.
21. Richardson P, McKenna W, Bristow M, et al. Report of the 1995 World Health Organization/International Society and Federation of Cardiology Task Force on the Definition and Classification of cardiomyopathies. *Circulation.* 1996;93:841–842.
22. Chiu C, Bagnall RD, Ingles J, et al. Mutations in Alpha-Actinin-2 Cause Hypertrophic Cardiomyopathy. *J Am Coll Cardiol.* 2010;55:1127–1135.
23. Harris KM, Spirito P, Maron MS, et al. Prevalence, clinical profile, and significance of left ventricular remodeling in the end-stage phase of hypertrophic cardiomyopathy. *Circulation.* 2006;114:216–225.
24. Konno T, Shimizu M, Ino H, et al. A novel mutation in the cardiac myosin-binding protein C gene is responsible for hypertrophic cardiomyopathy with severe ventricular hypertrophy and sudden death. *Cli Sci (Lond).* 2006;110:125–131.
25. Uchiyama K, Hayashi K, Fujino N, et al. Impact of QT Variables on clinical outcome of genotyped hypertrophic cardiomyopathy. *Ann Noninvasive Electrocardiol.* 2009;14:65–71.
26. Funada A, Konno T, Fujino N, et al. Impact of renin-angiotensin system polymorphisms on development of systolic dysfunction in hypertrophic cardiomyopathy. Evidence from a study of genotyped patients. *Circ J.* 2010;74:2674–2680.
27. CardioGenomics. http://cardiogenomics.med.harvard.edu/home. Accessed January 24, 2012.
28. Sakata K, Ino H, Fujino N, et al. Exercise-induced systolic dysfunction in patients with non-obstructive hypertrophic cardiomyopathy and mutations in the cardiac troponin genes. *Heart.* 2008;94:1281–1287.
29. Semsarian C, Ahmad I, Giewat M, et al. The L-type calcium channel inhibitor diltiazem prevents cardiomyopathy in a mouse model. *J Clin Invest.* 2002;109:1013–1020.
30. Ho CY, Lever HM, DeSanctis R, et al. Homozygous mutation in cardiac troponin T implications for hypertrophic cardiomyopathy. *Circulation.* 2000;102:1950–1955.
31. Richard P, Charron P, Leclercq C, et al. Homozygotes for a R869G mutation in the beta -myosin heavy chain gene have a severe form of familial hypertrophic cardiomyopathy. *J Mol Cell Cardiol.* 2000;32:1575–1583.
32. Richard P, Charron P, Carrier L, et al. EUROGENE Heart Failure Project. Hypertrophic cardiomyopathy: distribution of disease genes, spectrum of mutations, and implications for a molecular diagnosis strategy. *Circulation.* 2003;107:2227–2232.
33. Van Driest SL, Vasile VC, Ommen SR, et al. Myosin binding protein C mutations and compound heterozygosity in hypertrophic cardiomyopathy. *J Am Coll Cardiol.* 2004;44:1903–1910.
34. Ingles J, Doolan A, Chiu C, et al. Compound and double mutations in patients with hypertrophic cardiomyopathy: implications for genetic testing and counselling. *J Med Genet.* 2005;42:e59.
35. Kubo T, Kitaoka H, Okawa M, et al. Genetic screening and double mutation in Japanese patients with hypertrophic cardiomyopathy. *Circ J.* 2011;75:2654–2659.

Published online in Wiley Online Library (wileyonlinelibrary.com)
DOI:10.1002/clc.22082

Life Sciences 90 (2012) 619–628

Contents lists available at SciVerse ScienceDirect

Life Sciences

journal homepage: www.elsevier.com/locate/lifescie

Effect of persistent activation of phosphoinositide 3-kinase on heart

Shinichiro Niizuma [a,1], Yasutaka Inuzuka [a,1], Junji Okuda [a], Takao Kato [a], Tsuneaki Kawashima [a], Yodo Tamaki [a], Yoshitaka Iwanaga [a], Yuki Yoshida [b], Rie Kosugi [b], Kayo Watanabe-Maeda [b], Yoji Machida [b], Shingo Tsuji [c], Hiroyuki Aburatani [c], Tohru Izumi [b], Toru Kita [a], Takeshi Kimura [a], Tetsuo Shioi [a,*]

[a] Department of Cardiovascular Medicine, Graduate School of Medicine, Kyoto University, Kyoto 606-8507, Japan
[b] Department of Cardio-angiology, Kitasato University School of Medicine, Kanagawa 228-8555, Japan
[c] Genome Science Division, Research Center for Advanced Science and Technology, The University of Tokyo, Tokyo 153-8904, Japan

ARTICLE INFO

Article history:
Received 22 September 2011
Accepted 17 February 2012

Keywords:
Insulin
Phosphoinositide 3-kinase
Gene expression
Aging

ABSTRACT

Aims: Insulin/insulin-like growth factor-1 (IGF-1) signaling plays an important role in many biological processes. The class IA isoform of phosphoinositide 3-kinase (PI3K) is an important downstream effector of the insulin/IGF-1 signaling pathway. The aim of this study is to examine the effect of persistent activation of PI3K on gene expression and markers of cellular senescence in murine hearts.
Main methods: Transgenic mice expressing a constitutively active PI3K in a heart-specific manner were analyzed at the ages of 3 and 20 months. Effects of persistent activation of PI3K on gene expression were comprehensively analyzed using microarrays.
Key findings: Upon comprehensive gene expression profiling, the genes whose expression was increased included those for several heat shock chaperons. The amount and nuclear localization of a forkhead box O (FOXO) protein was increased. In addition, the gene expression of insulin receptor substrate-2 decreased, and that of phosphatase and tensin homolog deleted on chromosome ten (PTEN) increased, suggesting that the persistent activation of PI3K modified the expression of molecules of insulin/IGF-1 signaling. The expression of markers of cellular senescence, such as senescence-associated beta-galactosidase activity, cell cycle inhibitors, proinflammatory cytokines, and lipofuscin, did not differ between old wild-type and caPI3K mice.
Significance: The persistent activation of PI3K modified the expression of molecules of insulin/IGF-1 signaling pathway in a transgenic mouse line. Markers of cellular senescence were not changed in the aged mutant mice.

Introduction

Insulin/insulin-like growth factor (IGF)-1 signaling is a complex, highly integrated system and regulates different intracellular signaling pathways. Insulin/IGF-1 signaling regulates several important physiological processes, such as metabolism, growth, survival, differentiation, and aging (Kenyon, 2010). Class IA phosphoinositide 3-kinase (PI3K) is a lipid kinase, and an important downstream effector of insulin/IGF-1 signaling (Cantley, 2002). The enzyme is composed of a p85 regulatory subunit which binds to insulin receptor substrates (IRSs), and a p110 catalytic subunit. The association of p85 with IRS proteins increases the catalytic activity of the p110 subunit. The p85 subunit has two isoforms (p85α and β, and the p110 subunit has four isoforms (P110α, β, γ, and δ.

Insulin/IGF-1 signaling plays a key role in adaptations to changes in nutrient availability. Considering the system's importance in regulating cellular metabolism, multiple feedback mechanisms may exist to fine-tune it (Taniguchi et al., 2006). Loss of PI3K activity impairs glucose uptake and glycogen synthesis (Okada et al., 1994). Persistent activation of PI3K increased glucose uptake (Egawa et al., 2000). However, the insulin-induced increase in glucose uptake was blunted, and basal and insulin-induced glycogen synthesis was abolished by the continued activation of PI3K. The results indicate that the persistent activation of PI3K mimics some of the actions of insulin, but also induces a state of cellular insulin resistance (Egawa et al., 1999).

Previous studies have suggested that insulin/insulin-like growth factor-1 (IGF-1) signaling is important in aging (Kenyon, 2005). A vast amount of literature suggests that a decrease of insulin/IGF1 signaling in an appropriate range extends life-span in model organisms. However, very few studies have examined whether a gain of function of insulin/IGF1 signaling modifies aging (Vijg and Suh, 2005), probably because a genetic mutation that extends life span is considered more informative than a mutation that shortens it in experiments using smaller organisms, such as *Caenorhabditis elegans*

* Corresponding author at: Department of Cardiovascular Medicine, Graduate School of Medicine, Kyoto University, 54 Shogoin kawahara-cho, Sakyo-ku, Kyoto 606-8507, Japan. Tel.: +81 75 751 3670; fax: +81 75 751 3203.
E-mail address: tshioi@kuhp.kyoto-u.ac.jp (T. Shioi).
[1] These authors contributed equally to this paper.

0024-3205/$ – see front matter © 2012 Published by Elsevier Inc.
doi:10.1016/j.lfs.2012.02.010

and *Drosophila*, as these organisms may die earlier through mechanisms not related to aging.

PI3K plays a critical role in growth, metabolism, and stress resistance in the heart (McMullen et al., 2003; O'Neill et al., 2007; Shioi et al., 2000). We have reported that suppression of PI3K prevents many of the age-associated changes in heart tissue (Inuzuka et al., 2009). The aim of this study was to examine the effect of the constitutive activation of PI3K in animals. To this end, we performed a comprehensive gene expression analysis in hearts from a transgenic line expressing a constitutively active PI3K in a heart-specific manner. To examine the influence on a physiological process, we also analyzed the effect of persistent activation of PI3K on markers of cellular senescence in aged mice.

Materials and methods

Animals

Mutant mice

Transgenic mice expressing a constitutively active mutant form of the p110α PI3K isoform (caPI3K) were generated on the FVB background as described previously (Shioi et al., 2000). PI3K activity increased 6.5-fold in caPI3K transgenic mice compared with non-transgenic mice (Shioi et al., 2000). caPI3K mice and non-transgenic (NTg) littermates at 3 months and 20 to 24 months of age were euthanized without fasting and analyzed. The NTg mice of the current study were the same animals used in our previous report (Inuzuka et al., 2009). Therefore, the comparison between young and old NTg mice has already been reported, and this is clearly indicated in this paper.

Administration of rapamycin

Ten- to twelve-month-old male C57BL/6J mice were purchased from the Jackson Laboratory (Yokohama, Japan) (Inuzuka et al., 2009). Rapamycin (8 mg/kg/day; Sigma) or vehicle was administered intraperitoneally 3 times a week for 8 weeks.

Injection of IGF-1

Three- to six-month-old caPI3K transgenic mice or NTg mice were anesthetized with intraperitoneal injections of 2,2,2 tribromoethanol (Aldrich). IGF-1 (5 mg/kg) or the same volume of saline was intravenously injected via a jugular vein. Hearts from NTg and caPI3K transgenic mice were harvested 5 min after the injection and rapidly frozen in liquid nitrogen as described (Shioi et al., 2002).

Three-month-old male C57/BL6 mice were purchased from the Jackson Laboratory (Yokohama, Japan). Different doses of IGF-1 (1, 5, or 25 mg/kg) or saline were injected intravenously, and hearts were harvested 5 min after the injection.

Ventricular tissues were used for the biochemical and histological analyses. All animal experiments and methods were approved by the Animal Care and Use Committees of Kitasato University School of Medicine and Kyoto University Graduate School of Medicine.

Microarray analysis

Total RNA was prepared from ventricular tissues using TRIZol (Life Technologies). Total RNA was hybridized on a GeneChip® Mouse Genome 430 2.0 array (Affymetrix, Inc. Santa Clara, CA) at the Research Center for Advanced Science and Technology, The University of Tokyo as described (Inuzuka et al., 2009). The results of the microarray assay were analyzed using GeneSpring 7.31 (Agilent, Santa Clara, CA). Array data were normalized using the 50th percentile per chip. To identify significant differential expression between the groups, a Welch *t*-test with multiple testing correction was used. The Benjamini and Hochberg False Discovery Rate (FDR) was calculated (Reiner et al., 2003) and 0.05 was used for the cutoff value. Transcripts were selected and presented based on a change of more than 1.2 fold or less than 0.8 fold. The microarray data have been deposited in the Center for Information Biology Gene Expression Database repository under accession No.CBX72.

Quantitative RT-PCR

Total RNA was prepared from ventricular tissues using TRIzol (Life Technologies). Quantitative RT-PCR was performed as described (Inuzuka et al., 2009). The expression of Glyceraldehyde-3-phosphate dehydrogenase (GAPDH) did not differ among the four experimental groups based on the results of quantitative RT-PCR and hybridization signals from the microarray analysis (data not shown). The genes and primer sequences analyzed are listed in Supplemental Table S1.

Western blotting

Total protein was extracted from frozen ventricular tissue, resolved, and electrotransferred as described (Inuzuka et al., 2009). The primary antibodies used for Western blotting were FOXO1 (1:1000, Cell Signaling Technology, Beverly, MA), FOXO3a (1:1000, Cell Signaling Technology, Beverly, MA), pFOXO3a (1:1000, Cell Signaling Technology, Beverly, MA), pS6 (1:1000, Cell Signaling Technology, Beverly, MA), LC3 (1:1000, PM036, Medical & Biological Laboratories, Aichi, Japan), and GAPDH (1:2000, 6C5, Chemicon International, Temecula, CA).

Immunofluorescence analysis

Ventricular tissue was embedded in OCT compound, snapfrozen on dry ice, and stored at −70 °C. Samples were sectioned on a cryostat at 10 μm and then fixed for 5 min in paraformaldehyde at 4 °C. The sections were incubated with anti-FOXO1 antibody (rabbit IgG, Cell Signaling) at 4 °C overnight. Next, sections were incubated with fluorescent isothiocyanate-labeled anti-rabbit IgG and rhodamine-labeled phalloidin at room temperature for 30 min. Nuclei were stained using 4′,6-diamidino-2-phenylindole (DAPI). Sections were analyzed under a fluorescence microscope (Carl Zeiss, Oberkochen, Germany).

Senescence-associated β-gal activity

Fresh frozen ventricular tissue sections were analyzed for senescence-associated β-gal (SA β-gal) activity according to the manufacturer's directions (Cell Signaling Technology, Beverly, MA) as described (Inuzuka et al., 2009). Sections were also stained with DAPI to visualize nuclei, and the number of cells positive for SA β-gal activity was divided by the number of nuclei in the microscopic field.

Measurement of lipofuscin

Lipofuscin content was quantified as described (Inuzuka et al., 2009). The autofluorescence intensity at 485 nm was expressed as units/100 mg tissue.

Cardiac echocardiography

Echocardiography was performed as described (Inuzuka et al., 2009) under anesthesia, using 2-2-2 tribromoethanol (240 mg/kg, Wako Pure Chemical Industries).

Statistical analysis

All data are expressed as the mean ± SEM. Data were analyzed with a 2-way ANOVA, and various groups were analyzed with post hoc comparisons using the Tukey–Kramer test when a significant interaction between age and genotype was documented. A value of $P<0.05$ was considered significant.

Results

Effect of persistent PI3K activation on gene expression in heart

To determine the changes of gene expression associated with persistent activation of PI3K, the gene expression profile of heart tissue was analyzed using whole-genome microarrays (6 hearts for each group). The expression of 35,902 transcripts was examined. Some 168 transcripts (0.47%) changed significantly in caPI3K mice compared to NTg mice at 3 months of age. Fifty seven transcripts were up-regulated in their expression, and 111 were down-regulated (Tables 1-1, 1-2). The microarray analysis of individual genes revealed those with the largest increase to include the genes for several heart shock proteins (HSPs), such as HSP1-like, HSP1, HSPA1, HSP4-like, HSP90 and HSP110. Thus, we analyzed the expression of HSP mRNAs based on the microarray data. The expression of 6 of 11 HSP genes increased in caPI3K compared to NTg mice (Fig. 1A). HSPs play an important role in protein homeostasis by inhibiting protein misfolding as molecular chaperons (Barral et al., 2004). HSP90 and HSP110 have been shown to act as molecular chaperons and maintain protein homeostasis (Polier et al., 2008; Proctor and Lorimer, 2011). To confirm the results of the microarray analysis, we measured the amounts of HSP90 and HSP110 by quantitative RT-PCR. Levels of both HSP90 and HSP110 mRNA were increased in caPI3K mice compared to NTg mice at 3 months of age (Fig. 1B).

To examine the effect of the inhibition of insulin signaling on the gene expression of HSPs, we quantified the HSP90 and HSP110 mRNA expression in hearts from mice administered rapamycin for eight weeks (Fig. 1C). Rapamycin is a lipophilic macrolide, which was first identified as a fungicide isolated from the soil bacterium *Streptomyces hygroscopicus*. Target of rapamycin (TOR) was first discovered in budding yeast through an analysis of dominant mutations that are resistant to the cytotoxic effects of rapamycin (Kunz et al., 1993). Rapamycin inhibits the function of TOR by forming a complex with FK506-binding protein-12 (FKBP-12), which then binds to a conserved region located immediately upstream of the kinase domain of TOR (Schmelzle and Hall, 2000). TOR is an important downstream effector of PI3K (Hay and Sonenberg, 2004). The expression of the HSP90 and HSP110 genes was increased in rapamycin-treated mice compared with vehicle-treated mice.

Increased expression and nuclear localization in cardiomyocytes of the FOXO1 protein in caPI3K mice

The expression of HSP genes is regulated by several transcription factors (Tower, 2011). One of these is Forkhead box O (FOXO) (Hsu et al., 2003). FOXO proteins form a family that includes FOXO1, FOXO3, FOXO4, and FOXO6 and play important roles in cell growth, survival, and metabolism (Gross et al., 2009). Insulin/IGF-1 activates PI3K and AKT, a downstream serine/threonine kinase of PI3K, and AKT phosphorylates FOXOs at multiple sites leading to their exclusion from the nucleus and thus the inhibition of their function as a transcriptional regulator. The amount of FOXO1 was increased in caPI3K mice compared to NTg mice (Fig. 2A). On immunohistochemical analysis, the FOXO1 protein was found in small vessels in both mice. In addition, nuclei of cardiac myocytes were also positive for FOXO1 in caPI3K mice, but not in NTg mice (Fig. 2B).

Table 1-1
Genes significantly up-regulated in caPI3K mice compared to NTg mice at 3 months of age (FDR<0.05, more than 1.2 fold).

Systematic name	Gene symbol	Description	Young caPI3K vs young NTg	
			Fold change	*P*-value
BI499717	Hsp110	Heat shock protein 110	3.00	<0.01
BC011080	Arntl	Aryl hydrocarbon receptor nuclear translocator-like	2.44	<0.01
C77384	Hspca	Heat shock protein 90 kDa alpha (cytosolic), class A member 1	2.17	<0.01
AF425643	Rab40b	Rab40b, member RAS oncogene family	2.14	<0.01
NM_007669	Cdkn1a	Cyclin-dependent kinase inhibitor 1A (P21)	2.08	<0.01
NM_080728	Myh7	Myosin, heavy polypeptide 7, cardiac muscle, beta	2.02	<0.01
NM_013558	Hspa1l	Heat shock protein 1-like	1.99	<0.01
AI314028	P4ha1	Procollagen-proline, 2-oxoglutarate 4-dioxygenase (proline 4-hydroxylase), alpha 1 polypeptide	1.96	<0.01
AK003182	Myl1	Myosin, light polypeptide 1	1.85	<0.01
BM120737	Ahsa2	AHA1, activator of heat shock protein ATPase homolog 2	1.69	<0.01
AV152288	Clu	Clusterin	1.66	<0.01
BB371406	Fzd2	Frizzled homolog 2 (*Drosophila*)	1.62	<0.01
NM_019914	Mllt11	Myeloid/lymphoid or mixed-lineage leukemia (trithorax homolog, *Drosophila*); translocated to, 11	1.58	<0.01
BB360504	Dnaic1	Dynein, axonemal, intermediate chain 1	1.58	<0.01
NM_011020	Hspa4l	Heat shock protein 4 like	1.58	<0.01
AF047377	Hspb1	Heat shock protein 1	1.55	<0.01
AI839535	Mamdc1	MAM domain containing glycosylphosphatidylinositol anchor 2	1.52	<0.01
BF462185	Abat	4-Aminobutyrate aminotransferase	1.49	<0.01
AK013924	Cacybp	Calcyclin binding protein	1.44	<0.01
AK015389	Htatip2	HIV-1 tat interactive protein 2, homolog	1.42	<0.01
BI154147	Hsp90ab1	Heat shock protein 90 kDa alpha (cytosolic), class B member 1	1.41	<0.01
BB829192	St3gal5	ST3 beta-galactoside alpha-2,3-sialyl transferase 5	1.41	<0.01
AV321215	Ahsa1	Activator of heat shock protein ATPase homolog 1	1.40	<0.01
NM_016737	Stip1	Stress-induced phosphoprotein 1	1.40	<0.01
NM_133726	St13	Suppression of tumorigenicity 13	1.39	<0.01
AK006582	Calr3	Calreticulin 3	1.39	<0.01
BB480432	Pdlim3	PDZ and LIM domain 3	1.39	<0.01
BC025020	Mboat2	Membrane bound O-acyltransferase domain containing 2	1.38	<0.01
BI251808	Cyp1b1	Cytochrome P450, family 1, subfamily b, polypeptide 1	1.37	<0.01
BB216259	Cmya4	Unc-45 homolog B (*C. elegans*)	1.36	<0.01
BF682469	Cd8b1	CD8 antigen, beta chain 1	1.33	<0.01
BC016447	Creb3l1	cAMP responsive element binding protein 3-like 1	1.33	<0.01
BB451008	Dbh	Dopamine beta hydroxylase	1.30	<0.01
BB008667	Lman2l	Lectin, mannose-binding 2-like	1.24	<0.01
BB384493	Dcun1d3	DCN1, defective in cullin neddylation 1, domain containing 3 (*S. cerevisiae*)	1.23	<0.01
NM_009836	Psme4	Proteasome (prosome, macropain) activator subunit 4	1.23	<0.01
NM_009228	Snta1	Syntrophin, acidic 1	1.23	<0.01
NM_008303	Hspe1	Heat shock protein 1 (chaperonin 10)	1.22	<0.01

Persistent activation of PI3K modified the expression of genes related to insulin/IGF-1 signaling

The increase in the gene expression of HSP90 and HSP110 in rapamycin-treated animals is expected, since inhibiting insulin/IGF-1 signaling activates FOXOs. However, increased gene expression of HSPs associated with the increase in a FOXO protein and its nuclear localization in caPI3K mice is an unexpected finding. Then, we hypothesized that the constitutive activation of PI3K may modify the

Table 1-2
Genes significantly down-regulated in caPI3K mice compared to NTg mice at 3 months of age (FDR<0.05, less than 0.8 fold).

Gene bank	Gene symbol	Description	Young caPI3K vs young NTg	
			Fold change	*P*-value
NM_009052	Bex1	Brain expressed gene 1	0.17	<0.01
AW106920	Pah	Phenylalanine hydroxylase	0.43	<0.01
AF165166	Prnd	Prion protein dublet	0.46	<0.01
NM_010161	Evi2a	Ecotropic viral integration site 2a	0.46	<0.01
AF035830	Per2	Period homolog 2 (*Drosophila*)	0.46	<0.01
NM_053082	Tspan4	Tetraspanin 4	0.49	<0.01
BC024942	Prps2	Phosphoribosyl pyrophosphate synthetase 2	0.50	<0.01
BB129992	Hccs	Holocytochrome c synthetase	0.50	<0.01
NM_010832	Msl31	Male-specific lethal-3 homolog 1 (*Drosophila*)	0.51	<0.01
NM_011067	Per3	Period homolog 3 (*Drosophila*)	0.51	<0.01
BB327418	Arhgap9	Rho GTPase activating protein 9	0.52	<0.01
W91024	Hist1h2ae	Histone cluster 1, H2ae	0.55	<0.01
AF177664	Arhgap6	Rho GTPase activating protein 6	0.56	<0.01
NM_008332	Ifit2	Interferon-induced protein with tetratricopeptide repeats 2	0.61	<0.01
NM_010501	Ifit3	Interferon-induced protein with tetratricopeptide repeats 3	0.61	<0.01
AF477481	Cdt1	Chromatin licensing and DNA replication factor 1	0.62	<0.01
BB250384	Vcam1	Vascular cell adhesion molecule 1	0.63	<0.01
AF004833	Tfpi	Tissue factor pathway inhibitor	0.63	<0.01
NM_007631	Ccnd1	Cyclin D1	0.64	<0.01
NM_009477	Upp1	Uridine phosphorylase 1	0.64	<0.01
AK011892	Plcd3	Phospholipase C, delta 3	0.64	<0.01
AI326478	Igh-6	Immunoglobulin heavy chain 6 (heavy chain of IgM)	0.65	<0.01
NM_021364	Clec5a	C-type lectin domain family 5, member a	0.65	<0.01
BM238926	Cdk6	Cyclin-dependent kinase 6	0.66	<0.01
NM_009349	Inmt	Indolethylamine N-methyltransferase	0.66	<0.01
AJ131395	Col14a1	Procollagen, type XIV, alpha 1	0.66	<0.01
NM_022019	Dusp10	Dual specificity phosphatase 10	0.66	<0.01
AI324988	Mcm5	Minichromosome maintenance deficient 5, cell division cycle 46 (*S. cerevisiae*)	0.67	<0.01
BB781435	Nid2	Nidogen 2	0.67	<0.01
NM_025703	Tceal8	Transcription elongation factor A (SII)-like 8	0.67	<0.01
NM_011909	Usp18	Ubiquitin specific peptidase 18	0.68	<0.01
NM_134131	Tnfaip8	Tumor necrosis factor, alpha-induced protein 8	0.68	<0.01
AI122415	Evi2b	Ecotropic viral integration site 2b	0.68	<0.01
BG919998	Stk39	Serine/threonine kinase 39, STE20/SPS1 homolog (yeast)	0.68	<0.01
BB533323	Agtrl1	Angiotensin receptor-like 1	0.69	<0.01
BF454057	Kctd12b	Potassium channel tetramerisation domain containing 12b	0.70	<0.01
AY035889	Tlr7	Toll-like receptor 7	0.70	<0.01
NM_029612	Slamf9	SLAM family member 9	0.70	<0.01
BC020144	Dsg2	Desmoglein 2	0.71	<0.01
BB495006	Cdh19	Cadherin 19, type 2	0.72	<0.01
AV006122	Ndrg4	N-myc downstream regulated gene 4	0.72	<0.01
AI551199	Agtr1	Angiotensin II receptor, type 1a	0.72	<0.01
BB474208	Myom2	Myomesin 2	0.72	<0.01
NM_133838	Ehd4	EH-domain containing 4	0.73	<0.01
BC012653	Cx3cr1	Chemokine (C-X3-C) receptor 1	0.73	<0.01
NM_011584	Nr1d2	Nuclear receptor subfamily 1, group D, member 2	0.73	<0.01
AK008952	P2ry5	Purinergic receptor P2Y, G-protein coupled, 5	0.73	<0.01
NM_007705	Cirbp	Cold inducible RNA binding protein	0.74	<0.01
NM_009320	Slc6a6	Solute carrier family 6 (neurotransmitter transporter, taurine), member 6	0.74	<0.01
NM_021791	Doc2g	Double C2, gamma	0.74	<0.01
BC016398	Prkab1	Protein kinase, AMP-activated, beta 1 non-catalytic subunit	0.76	<0.01
NM_022024	Gmfg	Glia maturation factor, gamma	0.76	<0.01
AK004559	Cpne8	Copine VIII	0.76	<0.01
AI553394	Usp2	Ubiquitin specific peptidase 2	0.76	<0.01
NM_010145	Ephx1	Epoxide hydrolase 1, microsomal	0.77	<0.01
BG071079	Ptch1	Patched homolog 1	0.77	<0.01
NM_025809	Clec14a	C-type lectin domain family 14, member a	0.77	<0.01
BB015508	Jmjd1c	Jumonji domain containing 1C	0.78	<0.01
BM124337	Obscn	Obscurin, cytoskeletal calmodulin and titin-interacting RhoGEF	0.78	<0.01
M24849	Vim	Vimentin	0.78	<0.01
NM_013640	Psmb10	Proteasome (prosome, macropain) subunit, beta type 10	0.78	<0.01
BC004724	Fn1	Fibronectin 1	0.79	<0.01
NM_009012	Rad50	RAD50 homolog (*S. cerevisiae*)	0.79	<0.01
BC027246	Rfwd3	Ring finger and WD repeat domain 3	0.79	<0.01
NM_008211	H3f3b	H3 histone, family 3B	0.79	<0.01

insulin/IGF-1 signaling pathway itself. First, we examined the effect of persistent PI3K activation on the expression of genes related to insulin/IGF-1 signaling using the microarray data. Insulin receptor substrate-2 (IRS2) expression decreased in caPI3K mice. The expression of phosphatase and tensin homolog deleted on chromosome ten (PTEN), which acts to attenuate PI3K signaling, was increased in caPI3K mice (Fig. 3A). To confirm the microarray data, we measured the amounts of IRS2 and PTEN by quantitative RT-PCR. IRS2 mRNA was decreased in caPI3K mice compared to NTg mice (Fig. 3B). PTEN mRNA was increased in caPI3K mice compared to NTg mice (Fig. 3B).

Phosphorylation of PI3K downstream molecules

We analyzed the phosphorylation of downstream targets of PI3K in caPI3K mice (Fig. 4A). The IGF-1 injection increased the amount of phosphorylated FOXO3a and ribosomal S6 proteins in NTg mice. The amounts of phosphorylated FOXO3a and ribosomal S6 in saline-injected caPI3K mice were increased compared with those in saline-injected NTg mice. The amounts of phosphorylated FOXO3a and ribosomal S6 in IGF-1-injected caPI3K mice did not differ from those in IGF-1-injected NTg mice.

To examine whether S6 or FOXO3a was maximally phosphorylated in caPI3K, we injected different doses of IGF-1 into wild-type mice, and measured the amounts of phosphorylated S6 and FOXO3a. As indicated in Fig. 4B, the amounts did not differ between mice injected with 5 mg/kg of IGF-1 and mice injected with 25 mg/kg of IGF-1. For FOXO3a, the amount of phosphorylated FOXO in saline-injected caPI3K mice was comparable to that of IGF-1-injected NTg mice. Thus, it is likely that FOXO3a was maximally phosphorylated in caPI3K mice. For S6, although the phosphorylation level was more variable between mice, there was no significant difference between IGF-injected NTg mice and saline-injected caPI3K mice in the experimental conditions we used (Fig. 4A). In summary, it was likely that S6 and FOXO3a were phosphorylated at nearly maximal levels in caPI3K mice.

Expression of markers of cellular senescence in old caPI3K mice

One of the physiological processes in which insulin/IGF-1 signaling plays an important role is aging. Thus, we examined the effect of the persistent activation of PI3K on the expression of markers of cellular senescence (Sikora et al., 2011). The markers were increased in old NTg mice as reported (Inuzuka et al., 2009). The cells positive for SA β-gal staining did not differ between old NTg mice and old caPI3K mice (Fig. 5A, B). Among the cell cycle inhibitors, p16 and p19 had increased mRNA levels in old NTg mice compared to young

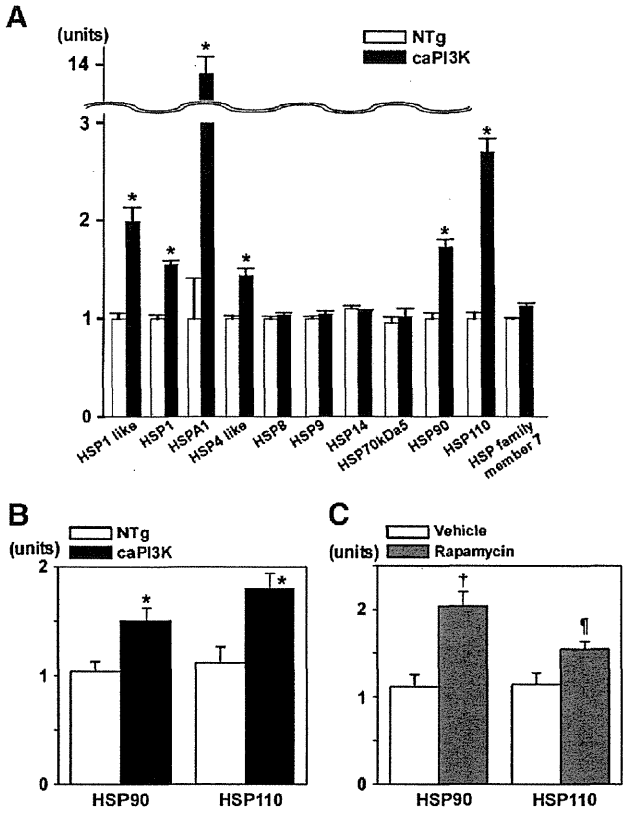

Fig. 1. Gene expression of heat shock proteins was increased in the heart of caPI3K mice. (A) The gene expression of heat shock proteins was analyzed on the basis of microarray data at three months of age (n = 6 for each group). Values are the mean ± SEM. *$P<0.05$ vs NTg mice. (B) The gene expression of HSP 90 and HSP 110 in three-month-old NTg mice and caPI3K mice was measured by quantitative RT-PCR (n = 10 to 11 for each group). Values are the mean ± SEM. *$P<0.05$ vs NTg mice. (C) Male C57BL/6J mice at ten to twelve months old were treated with rapamycin (n = 10) or vehicle (n = 8) for 8 weeks. The expression of HSP 90 and HSP110 mRNA was increased by rapamycin. Values are the mean ± SEM. †$P<0.05$ vs vehicle-treated mice. ¶$P = 0.06$ vs vehicle-treated mice.

NTg mice as reported (Inuzuka et al., 2009). The levels of mRNA for p16, p19, p53, and p21 did not differ between old NTg mice and old caPI3K mice (Fig. 6A). The gene expression of tumor necrosis factor-αTNF-α and interleukin 1βIL1β did not differ between old NTg and caPI3K mice either. Plasminogen activator inhibitor-1 (PAI-1) mRNA was increased by 1.73 ± 0.13 fold in old caPI3K mice compared with old NTg mice (Fig. 6A). The amount of lipofuscin in old caPI3K mice did not differ from that in old NTg mice (Fig. 6B).

The expression of HSP genes was increased in old caPI3K mice

Using a comprehensive analysis, we compared the gene expression between old NTg and old caPI3K mice (Tables 2-1, 2-2). The microarray analysis of individual genes showed those with the largest increase to include the genes for HSP1-like, HSP1, HSPA1, HSP4-like, HSP90, and HSP110.

The expression of genes of detoxification was increased in old caPI3K mice

Detoxification is another important mechanism to maintain protein homeostasis (Zimniak, 2008). According to the microarray analysis, the gene expression of phase 1 and phase 2 detoxification enzymes increased in old NTg mice as reported (Inuzuka et al., 2009). The expression of several detoxification enzymes was increased in old caPI3K mice compared to old NTg mice (Fig. 7A). We measured the amount of mRNA

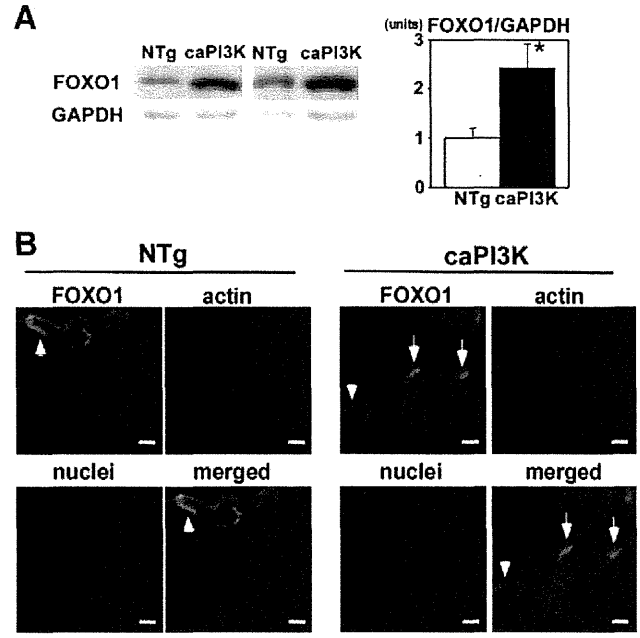

Fig. 2. FOXO1 protein increased and was located in nuclei of cardio myocytes in caPI3K mice. (A) Immunoblot analysis of FOXO1 in NTg mice and caPI3K mice. GAPDH was used as a loading control. Values are the mean ± SEM (n = 7 for each group). *$P<0.05$ vs NTg mice. (B) FOXO1 protein was located in small vessels (arrow heads) and in nuclei of cardiac myocytes in caPI3K mice (arrows) at three months of age. Bars represent 10 μm.

for glutathione *S*-transferase (GST) α2, as representative of detoxification enzymes, by quantitative RT-PCR. GSTα2 mRNA increased in old NTg mice compared to young NTg mice as described (Inuzuka et al.,

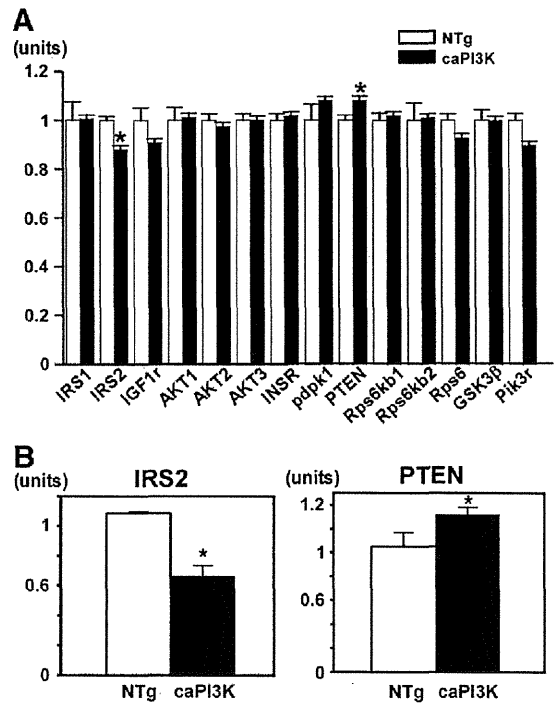

Fig. 3. Expression of genes related to PI3K signaling was modified in caPI3K mice. (A) The expression of genes involved PI3K signaling was analyzed on the basis of microarray data at three months of age (n = 6 for each group). (B) The gene expression of IRS2 and PTEN was measured by RT-PCR at three months of age (n = 10 to 11for each group). Values are the mean ± SEM. *$P<0.05$ vs NTg mice. IRS2; insulin receptor substrate-2, PTEN; phosphatase and tensin homolog deleted on chromosome ten.

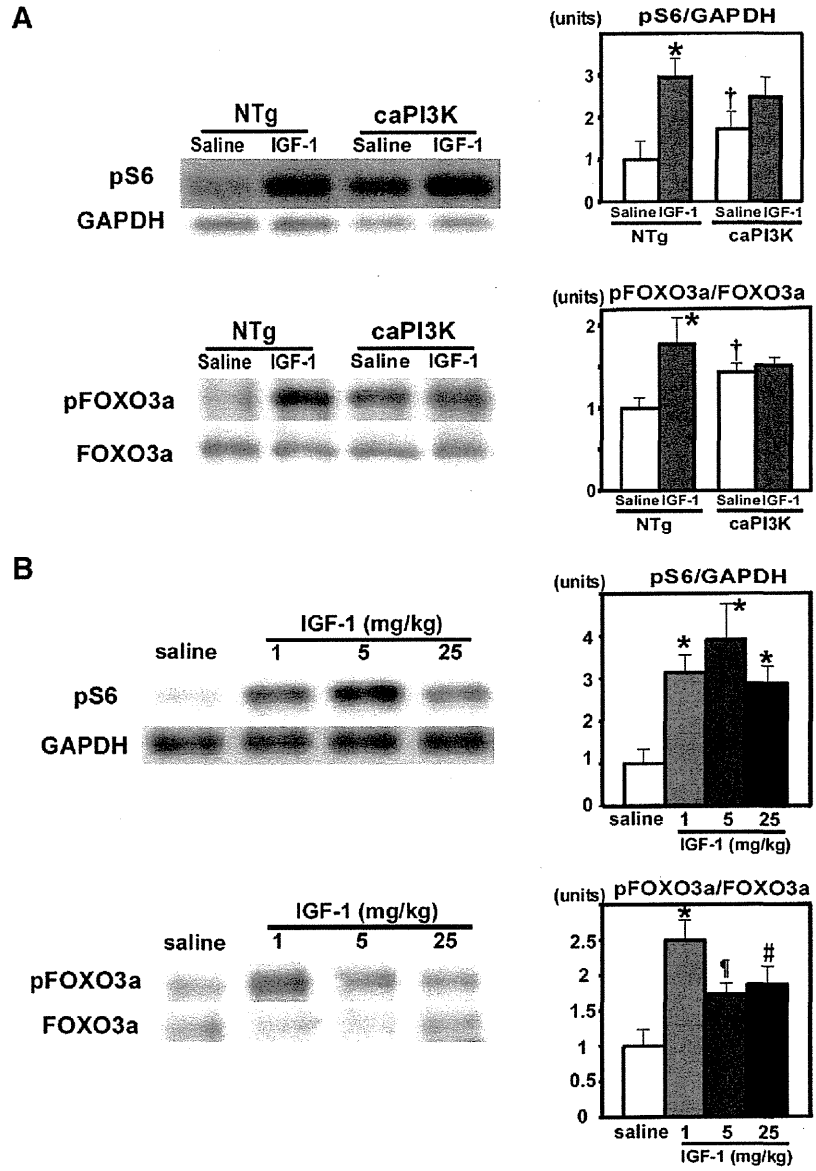

Fig. 4. Phosphorylation level of PI3K downstream molecules. (A). Immunoblot analysis of phosphorylated ribosomal S6 and FOXO3a in NTg mice and caPI3K mice injected with IGF-1. GAPDH was used as a loading control. caPI3K transgenic mice or NTg mice were injected with saline or 5 mg/kg of IGF-1. Each group represents four hearts. Values are the mean ± SEM.*$P<0.05$ vs mice of the same genotype; †$P<0.05$ vs mice of the same treatment (saline or IGF-1). (B.) Immunoblot analysis of phosphorylated ribosomal S6 and FOXO3a in wild-type mice injected with different doses of IGF-1. GAPDH was used as a loading control. Wild-type mice were injected with saline, or 1 mg/kg, 5 mg/kg, or 25 mg/kg of IGF-1. The amount of phosphorylated S6 and FOXO3a was not different between mice injected with 5 mg/kg of IGF-1 and mice injected with 1 mg/kg or 25 mg/kg of IGF-1. Each group represents four hearts. *$P<0.05$ vs mice injected with saline; ¶$P=0.09$ vs mice injected with saline; #$P=0.06$ vs mice injected with saline.

2009). GSTα2 mRNA increased in old caPI3K mice compared to old NTg mice (Fig. 7B).

Cardiac hypertrophy in old caPI3K transgenic mice

On echocardiographic examination, fractional shortening (FS), which represents cardiac systolic function, did not differ between young and old NTg mice. However, in old caPI3K mice, left ventricular diastolic diameter (LVDd) was increased and FS was slightly decreased (Table 3). Heart weight increased by 24% in old NTg mice compared with young NTg mice as reported (Inuzuka et al., 2009). The heart weight of caPI3K mice was increased compared to age-matched NTg mice by 22% (Table 4). Cardiac hypertrophy is typically associated with the transcriptional activation of several 'fetal' genes (Izumo et al., 1988). We analyzed the expression of atrial natriuretic factor (ANF), β-MHC, and α-skeletal actin by quantitative RT-PCR (Fig. 8). The gene expression of ANF, β-MHC, and α-skeletal actin was increased in old NTg mice compared to young NTg mice. The constitutive activation of PI3K enhanced the expression of β-MHC, and α-skeletal actin in old age. Intracellular calcium plays a key role in cardiac contraction and relaxation, and heart failure is associated with abnormal calcium handling. Many studies have shown decreased expression of cardiac sarco/endoplasmic reticulum calcium ATPase (SERCA) in failing heart (Berridge, 2006). The gene expression of SERCA 2a was decreased in old caPI3K mice compared to old NTg mice.

Discussion

Overexpression of the IGF-1 receptor promotes the growth of heart tissue (McMullen et al., 2004) and the expression of caPI3K increases heart size, indicating that persistent activation of PI3K mimics

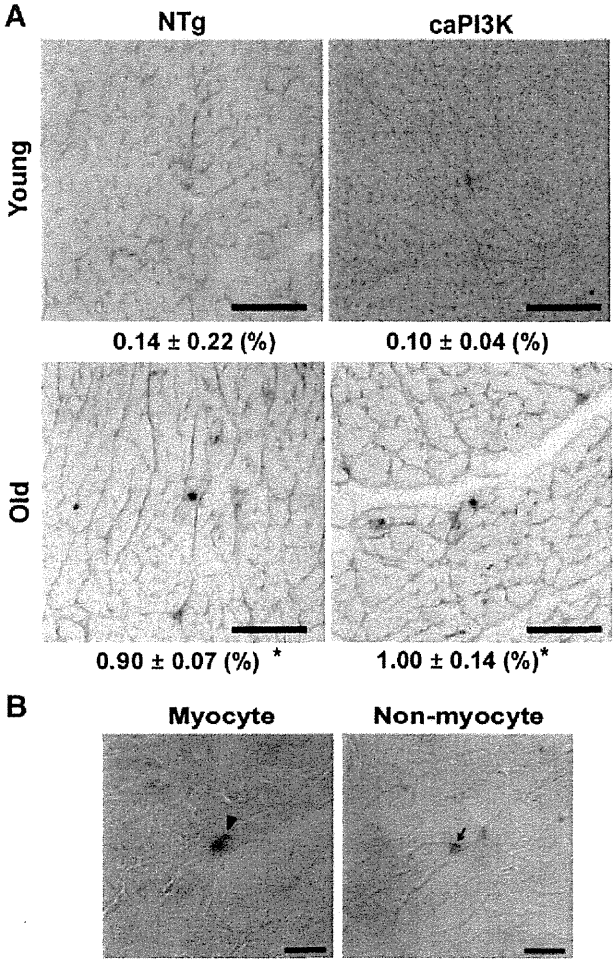

Fig. 5. The number of SA β-gal-positive cells was not changed in old caPI3K mice. (A) Senescence-associated beta-galactosidase (SA β-gal) activity was examined, and scattered cells positive for SA β-gal activity were observed in the myocardium of aged NTg mice. The number of SA β-gal-positive cells was counted, and divided by the number of nuclei in the microscopic fields. The number of SA β-gal-positive cells in old caPI3K mice did not differ from that in old NTg mice. Six hearts for each group were analyzed and the results were expressed as the mean ± SEM. Bars represent 50 μm. *$P<0.05$ vs younger mice of the same genotype. (B) At higher magnification, both cardiac myocytes (left panel) and non-myocytes (right panel) are positive for SA β-gal activity. Bars represent 25 μm.

the growth-promoting effect of the insulin/IGF-1 signaling pathway (Shioi et al., 2000). Upon a comprehensive gene expression analysis, the persistent PI3K activation increased the gene expression of heat shock chaperons. The level of a FOXO protein was increased and the protein was localized to nuclei in caPI3K mice, associated with the modified expression of genes related to insulin/IGF-1 signaling. The persistent PI3K activation did not modify markers of cellular senescence in the myocardium of aged mice.

The role of the insulin/IGF-1 pathway is conserved from worms to humans. The signaling system constitutes a key mechanism that has evolved to allow these organisms to adapt to changes in nutrient availability. Considering its importance to many biological processes, such as glucose homeostasis, cell growth, differentiation, and aging, it is plausible that multiple feedback mechanisms exist to fine tune the signaling module. Suppression of insulin/IGF-1 signaling attenuated age-related disease progression in a model of Alzheimer disease in mice (Cohen et al., 2009). Interestingly, long-term administration of IGF-1 also attenuated Alzheimer disease in mice (Carro et al., 2002). High plasma IGF-1 levels can lead to reduced IGF-1 signaling in centenarians, supporting the idea that feedback loops regulate the insulin/IGF-1 pathway in humans (Suh et al., 2008). Several feedback mechanisms exist in insulin/IGF-1 signaling, both transcriptional and post-transcriptional (Cohen and Dillin, 2008). Persistent activation of PI3K induces degradation of the IRS1 protein by ubiquitination, and causes a state of cellular insulin resistance (Egawa et al., 1999, 2000). Tuberous sclerosis complex (TSC) 1 and 2 are negative regulators of the insulin/IGF-1 signaling pathway, and their deletion decreases mRNA and protein levels of IRS1 and IRS2 (Shah et al., 2004). Ribosomal S6 kinase 1 (S6K) lies downstream of the insulin/IGF-1 signaling pathway and its activity is positively regulated by insulin or IGF-1. S6K1 phosphorylates IRS1 at S307 and S632 and inhibits insulin-induced Akt phosphorylation, making a negative feedback loop (Um et al., 2004).

The increase of PTEN or decrease of IRS2 mRNAs was modest. However, endothelial specific PTEN heterozygous knockout mice showed increased tumor angiogenesis (Hamada et al., 2005). Brain specific IRS2 heterozygous knockout mice showed increased life span (Taguchi et al., 2007). Thus, a mild difference in the expression of PTEN or IRS2 might be biologically significant if the change was prolonged in the aging process.

HSPs play a pivotal role in protein homeostasis by assisting protein folding, maintaining protein integrity, and mediating the clearance of misfolded proteins. Transcriptome analyses of *C. elegans* identified that HSPs are also regulated by DAF-16, a homolog of FOXOs (Hsu et al., 2003). In this study, increased expression of HSPs was associated

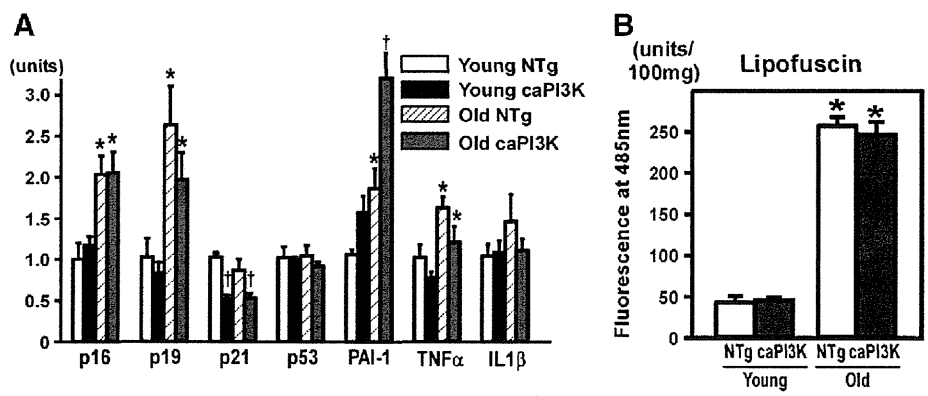

Fig. 6. Markers of cellular senescence were not different between old NTg mice and caPI3K mice. (A) The gene expression of cell cycle inhibitors and inflammation-related molecules was examined by quantitative RT-PCR (n = 10 to 11 for each group). The mean value for young NTg mice was expressed as 1 unit. PAI-1; plasminogen activator inhibitor-1, TNF-α; tumor necrosis factor-α, IL1β; interleukin 1β. Values are the mean ± SEM. *$P<0.05$ vs younger mice of the same genotype, †$P<0.05$ vs NTg mice of the same age. (B) Lipofuscin was extracted from heart tissue in a chloroform-methanol mixture and evaluated in a fluorescence spectrofluorometer. Autofluorescence at 485 nm was compared between the groups (n = 6 for each group). The age-associated increase in autofluorescence did not differ between old NTg mice and old caPI3K mice. Values are the mean ± SEM. *$P<0.05$ vs younger mice of the same genotype.

Table 2-1
Genes significantly up-regulated in caPI3K mice compared to NTg mice at 20 months of age (FDR<0.05, more than 1.2 fold).

Gene bank	Gene symbol	Description	Old caPI3K vs old NTg	
			Fold change	*P*-value
AW763765	Hspa1a	Heat shock protein 1A	10.51	<0.01
M12573	Hspa1b	Heat shock protein 1B	7.78	<0.01
AK003182	Myl1	Myosin, light polypeptide 1	3.66	<0.01
BG067039	Amot	Angiomotin	3.38	<0.01
NM_013558	Hspa1l	Heat shock protein 1-like	3.30	<0.01
BB477214	Masp1	Mannan-binding lectin serine peptidase 1	2.86	<0.01
BB359521	FIGF	C-fos induced growth factor	2.76	<0.01
AI314028	P4ha1	Procollagen-proline, 2-oxoglutarate 4-dioxygenase (proline 4-hydroxylase), alpha 1 polypeptide	2.70	<0.01
BI499717	Hsp110	Heat shock protein 110	2.62	<0.01
AI326984	Mybpc2	Myosin binding protein C, fast-type	2.55	<0.01
BB368452	Edn3	Endothelin 3	2.54	<0.01
NM_009813	Casq1	Calsequestrin 1	2.45	<0.01
NM_008871	Serpine1	Serine (or cysteine) peptidase inhibitor, clade E, member 1	2.35	<0.01
AV245981	Igsf1	Immunoglobulin superfamily, member 1	2.28	<0.01
BE988775	Rtn4	Reticulon 4	2.28	<0.01
BF225802	Igfbp5	Insulin-like growth factor binding protein 5	2.20	<0.01
C77384	Hspca	Heat shock protein 90 kDa alpha (cytosolic), class A member 1	2.05	<0.01
BB151516	Prkag3	Protein kinase, AMP-activated, gamma 3 non-catatlytic subunit	2.00	<0.01
BC009165	Thrsp	Thyroid hormone responsive SPOT14 homolog (Rattus)	1.93	<0.01
NM_009808	Casp12	Caspase 12	1.92	<0.01
NM_008597	Mgp	Matrix Gla protein	1.90	<0.01
L38990	Gck	Glucokinase	1.86	<0.01
NM_080451	Synpo2	Synaptopodin 2	1.83	<0.01
BB627486	Nova1	Neuro-oncological ventral antigen 1	1.80	<0.01
BI220012	Serpinh1	Serine (or cysteine) peptidase inhibitor, clade H, member 1	1.77	<0.01
BG793484	Ankrd23	Ankyrin repeat domain 23	1.64	<0.01
NM_008317	Hyal1	Hyaluronoglucosaminidase 1	1.63	<0.01
U03561	Hspb1	Heat shock protein 1	1.63	<0.01
NM_013492	Clu	Clusterin	1.56	<0.01
BI154147	Hsp90ab1	Heat shock protein 90 kDa alpha (cytosolic), class B member 1	1.56	<0.01
BC022922	Paqr7	Progestin and adipoQ receptor family member VII	1.54	<0.01
BE630020	Prnp	Prion protein	1.54	<0.01
BB797871	DACT3	Dapper homolog 3, antagonist of beta-catenin	1.52	<0.01
BE944771	Prkab2	Protein kinase, AMP-activated, beta 2 non-catalytic subunit	1.50	<0.01
AK003859	Rtn4	Reticulon 4	1.49	<0.01
BC014870	Parp3	Poly (ADP-ribose) polymerase family, member 3	1.47	<0.01
BC006722	Hspa8	Heat shock protein 8	1.45	<0.01
AL024092	Cct3	Chaperonin subunit 3 (gamma)	1.45	<0.01
AV317107	Senp2	SUMO/sentrin specific peptidase 2	1.44	<0.01
NM_015825	Sh3bgr	SH3-binding domain glutamic acid-rich protein	1.44	<0.01
BC017161	Dnajb4	DnaJ (Hsp40) homolog, subfamily B, member 4	1.41	<0.01
AF022072	Grb10	Growth factor receptor bound protein 10	1.40	<0.01
NM_019682	Dynll1	Dynein light chain LC8-type 1	1.40	<0.01
BC002187	Park7	Parkinson disease (autosomal recessive, early onset) 7	1.39	<0.01
BM195254	Psme4	Proteasome (prosome, macropain) activator subunit 4	1.37	<0.01
BG065255	Pou3f1	POU domain, class 3, transcription factor 1	1.31	<0.01
NM_009964	Cryab	Crystallin, alpha B	1.30	<0.01
M14222	Ctsb	Cathepsin B	1.28	<0.01
AV231357	PTPN3	Protein tyrosine phosphatase, non-receptor type 3	1.28	<0.01

Table 2-2
Genes significantly down-regulated in caPI3K mice compared to NTg mice at 20 months of age (FDR<0.05, less than 0.8 fold).

Gene bank	Gene symbol	Description	Old caPI3K vs old NTg	
			Fold change	*P*-value
NM_009052	Bex1	Brain expressed gene 1	0.10	<0.01
AW106920	Pah	Phenylalanine hydroxylase	0.31	<0.01
BE848253	Cenpf	Centromere protein F	0.32	<0.01
BC024942	Prps2	Phosphoribosyl pyrophosphate synthetase 2	0.42	<0.01
NM_013530	Gnb3	Guanine nucleotide binding protein, beta 3	0.42	<0.01
BB313865	A930041G11Rik	Von Willebrand factor C domain containing 2	0.44	<0.01
BB327418	Arhgap9	Rho GTPase activating protein 9	0.44	<0.01
AF004833	Tfpi	Tissue factor pathway inhibitor	0.45	<0.01
BC024112	Aldob	Aldolase 2, B isoform	0.49	<0.01
BG063249	Cmtm8	CKLF-like MARVEL transmembrane domain containing 8	0.55	<0.01
BB752393	Casp7	Caspase 7	0.55	<0.01
BB474208	Myom2	Myomesin 2	0.56	<0.01
AA408168	Dsg2	Desmoglein 2	0.57	<0.01
AW060663	Ift81	Intraflagellar transport 81 homolog (*Chlamydomonas*)	0.59	<0.01
BB043465	Slc2a12	Solute carrier family 2 (facilitated glucose transporter), member 12	0.61	<0.01
AK017352	Amtn	Amelotin	0.63	<0.01
BB745167	Ppargc1a	Peroxisome proliferative activated receptor, gamma, coactivator 1 alpha	0.63	<0.01
BB462269	Ttll1	Tubulin tyrosine ligase-like 1	0.63	<0.01
BF322712	Bdh1	3-Hydroxybutyrate dehydrogenase, type 1	0.64	<0.01
NM_011797	Car14	Carbonic anhydrase 14	0.66	<0.01
BC019521	Zfyve21	Zinc finger, FYVE domain containing 21	0.66	<0.01
BB426194	Tac1	Tachykinin 1	0.67	<0.01
AY059394	Cadm4	Cell adhesion molecule 4	0.70	<0.01
BQ176713	A2bp1	Transcribed locus	0.71	<0.01
NM_010176	Fah	Fumarylacetoacetate hydrolase	0.73	<0.01
AF020737	Fgf13	Fibroblast growth factor 13	0.76	<0.01
NM_016675	Cldn2	Claudin 2	0.76	<0.01
NM_025798	Hint3	Histidine triad nucleotide binding protein 3	0.77	<0.01
NM_010887	Ndufs4	NADH dehydrogenase (ubiquinone) Fe–S protein 4	0.78	<0.01
AK011936	Ablim1	Actin-binding LIM protein 1	0.78	<0.01
NM_011288	Mrpl23	Mitochondrial ribosomal protein L23	0.79	<0.01

with increased levels and nuclear localization of the FOXO1 protein. It is well established that insulin/IGF-1 signaling phosphorylates FOXOs via AKT, and causes the nuclear export and inactivation of FOXOs. However, the distribution of FOXO is known to be regulated by multiple mechanisms other than phosphorylation, such as acetylation and ubiquitination (Daitoku and Fukamizu, 2007). The mechanism by which FOXO was localized to nuclei in this study remains to be clarified.

The finding that persistent activation of PI3K did not modify markers of cellular senescence needs to be interpreted with caution, since it was based on the observation of a single transgenic line. However, we believe that the result is of physiological relevance, because the expression of the transgene promoted heart growth (Shioi et al., 2000), and protected the heart against pressure-overload (McMullen et al., 2007). We have reported that impaired protein homeostasis is a characteristic of age-related changes of the heart. Thus, increased levels of heat shock chaperons in young and old mice, and increased detoxification in old age, may attenuate the potential cellular senescence-promoting effect of persistent PI3K activation at the cellular level. Alternatively, aging is likely to occur as a mosaic of multiple mechanisms, and different mechanisms might act under different experimental conditions.

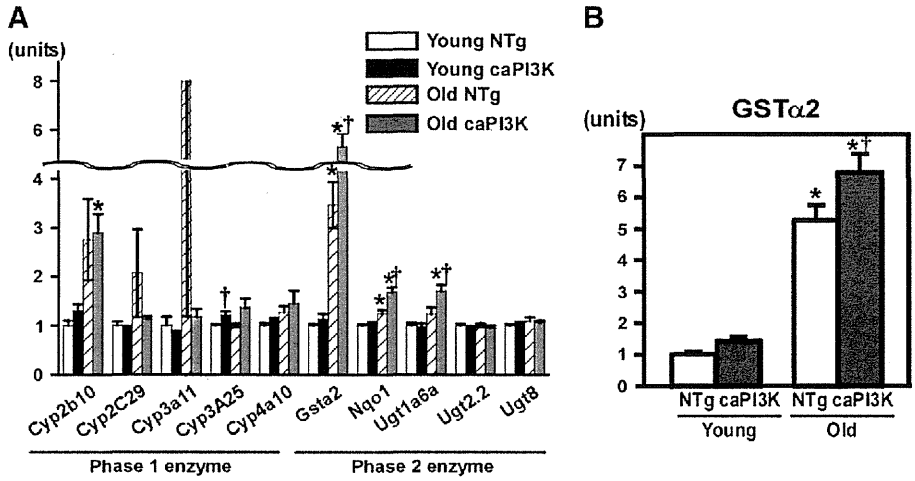

Fig. 7. Expression of detoxification-related genes was increased in old caPI3K mice. (A) Gene expression of phase 1 and phase 2 detoxification enzymes was analyzed on the basis of microarray data (n = 6 for each group). (B) The gene expression of GSTα2 was measured by quantitative RT-PCR (n = 10 to 11for each group). GSTα2; Glutathione S-transferase alpha 2. Values are the mean ± SEM. *P<0.05 vs younger mice of the same genotype; †P<0.05 vs NTg mice of the same age.

In the current study, p21 was decreased in young and old caPI3K mice. p21 was originally discovered as an inhibitor of cyclin-dependent protein kinases (Jung et al., 2010). In addition, p21 is a target of the p53 tumor suppressor. p21 is implicated in multiple biological processes including cell cycle, cell death, DNA repair, and aging. p21 null mice are phenotypically normal (Deng et al., 1995). However, deletion of p21 prevents premature aging in mice (Choudhury et al., 2007). Thus, decreased p21 also might counteract the potential pro-senescence effect of persistent PI3K activation.

Our findings confirmed a previous report that persistent local expression of IGF-1 initially induced physiological hypertrophy, which progressed to a pathological state later in life (Delaughter et al., 1999). Although the mechanism by which cardiac function mildly deteriorated in old caPI3K mice is unknown, it is likely that enhancement of the age-associated increase of heart size by caPI3K caused cardiac hypertrophy beyond a physiological level. Thus, we speculate that the pro-senescence effect of the constitutively active PI3K was

Table 3
Echocardiographic analysis of young and old caPI3K mice.

	Young		Old	
	NTg (n = 10)	caPI3K (n = 10)	NTg (n = 10)	caPI3K (n = 10)
Heart rate (bpm)	520 ± 13	527 ± 12	512 ± 10	498 ± 12
LV diastolic diameter (mm)	3.73 ± 0.03	3.75 ± 0.05	4.15 ± 0.04*	4.19 ± 0.07*
LV systolic diameter (mm)	2.02 ± 0.03	2.05 ± 0.04	2.29 ± 0.03*	2.40 ± 0.05*†
FS (%)	46.0 ± 0.5	45.4 ± 0.4	44.7 ± 0.9	42.6 ± 0.6*†
Posterior wall thickness (mm)	0.66 ± 0.02	0.72 ± 0.02	0.78 ± 0.03*	0.83 ± 0.02*

Values are expressed as the mean ± SEM. NTg, non-transgenic mice; caPI3K, constitutively active PI3K transgenic mice; bpm, beats per minute; LV, left ventricular; FS, fractional shortening. *P<0.05 vs younger mice of the same genotype. †P<0.05 vs NTg mice at the same age. Young groups represent three-month old mice, and old groups represent 20 to 24-month old mice.

Table 4
Heart weight and lung weight of young and old caPI3K mice.

	Young		Old	
	NTg (n = 10)	caPI3K (n = 10)	NTg (n = 13)	caPI3K (n = 11)
Body weight (BW, g)	32.0 ± 0.5	31.6 ± 0.8	37.9 ± 1.0*	37.4 ± 0.9*
Tibial length (TL, mm)	17.3 ± 0.1	17.2 ± 0.1	18.1 ± 0.1*	18.4 ± 0.2*
Heart weight (HW, mg)	122 ± 2	144 ± 3†	162 ± 5*	197 ± 3*†
Lung weight (LW, mg)	171 ± 4	166 ± 4	185 ± 5	195 ± 7*
HW/BW (mg/g)	3.81 ± 0.07	4.57 ± 0.10†	4.32 ± 0.19*	5.29 ± 0.12*†
LW/BW (mg/g)	5.35 ± 0.14	4.99 ± 0.16	4.93 ± 0.17	5.26 ± 0.26
HW/TL (mg/mm)	7.05 ± 0.10	8.45 ± 0.19†	8.77 ± 0.28*	10.75 ± 0.18*†
LW/TL (mg/mm)	9.90 ± 0.26	9.12 ± 0.23	10.2 ± 0.27	10.6 ± 0.38

Values are expressed as the mean ± SEM. NTg, non-transgenic mice; caPI3K, constitutively active PI3K transgenic mice. *P<0.05 vs young mice of the same genotype. †P<0.05 vs NTg mice at the same age.
Young groups represent three month-old mice, and old groups represent 20 to 24 month-old mice.

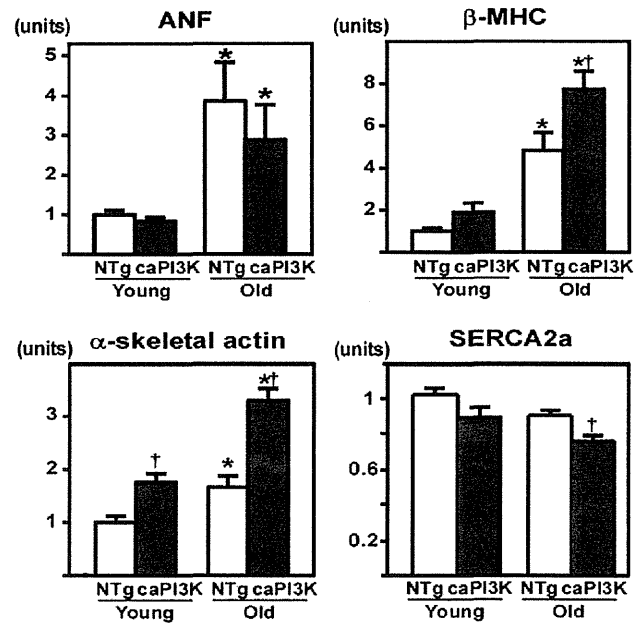

Fig. 8. Expression of markers of cardiac hypertrophy increased in old caPI3K mice. The expression of fetal genes was examined by quantitative RT-PCR (n = 10 to 11 for each group). The mean value for young NTg mice was expressed as 1 unit. Gene expression of atrial natriuretic factor (ANF), β-myosin heavy chain MHC), α-skeletal actin and sarco/endoplasmic reticulumcalcium ATPase (SERCA) 2a was analyzed using quantitative RT-PCR. Values are the mean ± SEM. *P<0.05 vs younger mice of the same genotype; †P<0.05 vs NTg mice of the same age.

attenuated by multiple compensatory mechanisms at the cellular level, but an excessive increase in heart size caused a mild impairment of heart function at the organ level. Alternatively, other mechanisms that were not represented by the changes in markers of cellular senescence may promote aging at the level of an organ.

Conflict of interest statement

The authors declare that there are no conflicts of interest.

Conclusion

The persistent activation of PI3K modified the expression of molecules of insulin/IGF-1 signaling in a transgenic mouse line. Markers of cellular senescence were not changed in the aged mutant mice.

Supplementary materials related to this article can be found online at doi:10.1016/j.lfs.2012.02.010.

Acknowledgments

Grants from the Japan Society for the Promotion of Science, the Japan Heart Foundation, the Japan Foundation of Cardiovascular Research, NOVARTIS Foundation for the Promotion of Science, the Mochida Memorial Foundation for Medical and Pharmaceutical Research, the Takeda Medical Research Foundation, the Kanagawa Nanbyo Foundation, the Takeda Science Foundation, and the Vehicle Racing Commemorative Foundation.

References

Barral JM, Broadley SA, Schaffar G, Hartl FU. Roles of molecular chaperones in protein misfolding diseases. Semin Cell Dev Biol 2004;15:17–29.
Berridge MJ. Remodelling Ca^{2+} signalling systems and cardiac hypertrophy. Biochem Soc Trans 2006;34:228–31.
Cantley LC. The phosphoinositide 3-kinase pathway. Science 2002;296:1655–7.
Carro E, Trejo JL, Gomez-Isia T, LeRoith D, Torres-Aleman I. Serum insulin-like growth factor 1 regulates brain amyloid-beta levels. Nat Med 2002;8:1390–7.
Choudhury AR, Ju Z, Djojosubroto MW, Schienke A, Lechel A, Schaetzlein S, et al. Cdkn1a deletion improves stem cell function and lifespan of mice with dysfunctional telomeres without accelerating cancer formation. Nat Genet 2007;39: 99-105.
Cohen E, Dillin A. The insulin paradox: aging, proteotoxicity and neurodegeneration. Nat Rev Neurosci 2008;9:759–67.
Cohen E, Paulsson JF, Blinder P, Burstyn-Cohen T, Du D, Estepa G, et al. Reduced IGF-1 signaling delays age-associated proteotoxicity in mice. Cell 2009;139:1157–69.
Daitoku H, Fukamizu A. FOXO transcription factors in the regulatory networks of longevity. J Biochem 2007;141:769–74.
Delaughter MC, Taffet GE, Fiorotto ML, Entman ML, Schwartz RJ. Local insulin-like growth factor I expression induces physiologic, then pathologic, cardiac hypertrophy in transgenic mice. FASEB J 1999;13:1923–9.
Deng C, Zhang P, Harper JW, Elledge SJ, Leder P. Mice lacking p21CIP1/WAF1 undergo normal development, but are defective in G1 checkpoint control. Cell 1995;25(82):675–84.
Egawa K, Sharma PM, Nakashima N, Huang Y, Huver E, Boss GR, et al. Membrane-targeted phosphatidylinositol 3-kinase mimics insulin actions and induces a state of cellular insulin resistance. J Biol Chem 1999;274:14306–14.
Egawa K, Nakashima N, Sharma PM, Maegawa H, Nagai Y, Kashiwagi A, et al. Persistent activation of phosphatidylinositol 3-kinase causes insulin resistance due to accelerated insulin-induced insulin receptor substrate-1 degradation in 3T3-L1 adipocytes. Endocrinology 2000;141:1930–5.
Gross DN, Wan M, Birnbaum MJ. The role of FOXO in the regulation of metabolism. Curr Diab Rep 2009;9:208–14.
Hamada K, Sasaki T, Koni PA, Natsui M, Kishimoto H, Sasaki J, et al. The PTEN/PI3K pathway governs normal vascular development and tumor angiogenesis. Genes Dev 2005;19:2054–65.
Hay N, Sonenberg N. Upstream and downstream of mTOR. Genes Dev 2004;18: 1926–45.
Hsu AL, Murphy CT, Kenyon C. Regulation of aging and age-related disease by DAF-16 and heat-shock factor. Science 2003;300:1142–5.
Inuzuka Y, Okuda J, Kawashima T, Kato T, Niizuma S, Tamaki Y, et al. Suppression of phosphoinositide 3kinase prevents cardiac aging in mice. Circulation 2009;120: 1695–703.
Izumo S, Nadal-Ginard B, Mahdavi V. Protooncogene induction and reprogramming of cardiac gene expression produced by pressure overload. Proc Natl Acad Sci U S A 1988;85:339–43.
Jung YS, Qian Y, Chen X. Examination of the expanding pathways for the regulation of p21 expression and activity. Cell Signal 2010;22:1003–12.
Kenyon C. The plasticity of aging: insights from long-lived mutants. Cell 2005;120: 449–60.
Kenyon C. The genetics of ageing. Nature 2010;464:504–12.
Kunz J, Henriquez R, Schneider U, Deuter-Reinhard M, Movva NR, Hall MN. Target of rapamycin in yeast, TOR2, is an essential phosphatidylinositol kinase homolog required for G1 progression. Cell 1993;73:585–96.
McMullen JR, Shioi T, Zhang L, Tarnavski O, Sherwood MC, Kang PM, et al. Phosphoinositide 3-kinase(p110alpha) plays a critical role for the induction of physiological, but not pathological, cardiac hypertrophy. Proc Natl Acad Sci U S A 2003;100: 12355–60.
McMullen JR, Shioi T, Huang WY, Zhang L, Tarnavski O, Bisping E, et al. The insulin-like growth factor 1 receptor induces physiological heart growth via the phosphoinositide 3-kinase(p110alpha) pathway. J Biol Chem 2004;279:4782–93.
McMullen JR, Amirahmadi F, Woodcock EA, Schinke-Braun M, Bouwman RD, Hewitt KA, et al. Protective effects of exercise and phosphoinositide 3-kinase (p110alpha) signaling in dilated and hypertrophic cardiomyopathy. Proc Natl Acad Sci U S A 2007;104:612–7.
Okada T, Kawano Y, Sakakibara T, Hazeki O, Ui M. Essential role of phosphatidylinositol 3-kinase in insulin-induced glucose transport and antilipolysis in rat adipocytes. Studies with a selective inhibitor wortmannin. J Biol Chem 1994;269: 3568–73.
O'Neill BT, Kim J, Wende AR, Theobald HA, Tuinei J, Buchanan J, et al. A conserved role for phosphatidylinositol 3-kinase but not Akt signaling in mitochondrial adaptations that accompany physiological cardiac hypertrophy. Cell Metab 2007;6: 294–306.
Polier S, Dragovic Z, Hartl FU, Bracher A. Structural basis for the cooperation of hsp70 and hsp110 chaperones in protein folding. Cell 2008;133:1068–79.
Proctor CJ, Lorimer IA. Modelling the role of the hsp70/hsp90 system in the maintenance of protein homeostasis. PLoS One 2011;6:e22038.
Reiner A, Yekutieli D, Benjamini Y. Identifying differentially expressed genes using false discovery rate controlling procedures. Bioinformatics 2003;19:368–75.
Schmelzle T, Hall MN. TOR, a central controller of cell growth. Cell 2000;103:253–62.
Shah OJ, Wang Z, Hunter T. Inappropriate activation of the tsc/rheb/mtor/s6k cassette induces irs1/2 depletion, insulin resistance, and cell survival deficiencies. Curr Biol 2004;14:1650–6.
Shioi T, Kang PM, Douglas PS, Hampe J, Yballe CM, Lawitts J, et al. The conserved phosphoinositide 3-kinase pathway determines heart size in mice. EMBO J 2000;19: 2537–48.
Shioi T, McMullen JR, Kang PM, Douglas PS, Obata T, Franke TF, et al. Akt/protein kinase B promotes organ growth in transgenic mice. Mol Cell Biol 2002;22:2799–809.
Sikora E, Arendt T, Bennett M, Narita M. Impact of cellular senescence signature on ageing research. Ageing Res Rev 2011;10:146–52.
Suh Y, Atzmon G, Cho MO, Hwang D, Liu B, Leahy DJ, et al. Functionally significant insulin-like growth factor I receptor mutations in centenarians. Proc Natl Acad Sci U S A 2008;105:3438–42.
Taguchi A, Wartschow LM, White MF. Brain IRS2 signaling coordinates life span and nutrient homeostasis. Science 2007;317:369–72.
Taniguchi CM, Emanuelli B, Kahn CR. Critical nodes in signalling pathways: insights into insulin action. Nat Rev Mol Cell 2006;7:85–96.
Tower J. Heat shock proteins and *Drosophila* aging. Exp Gerontol 2011;46:355–62.
Um SH, Frigerio F, Watanabe M, Picard F, Joaquin M, Sticker M, et al. Absence of S6K1 protects against age- and diet-induced obesity while enhancing insulin sensitivity. Nature 2004;431:200–5.
Vijg J, Suh Y. Genetics of longevity and aging. Annu Rev Med 2005;56:193–212.
Zimniak P. Detoxification reactions: relevance to aging. Ageing Res Rev 2008;7: 281–300.

LETTER

doi:10.1038/nature10992

Mitochondrial DNA that escapes from autophagy causes inflammation and heart failure

Takafumi Oka[1], Shungo Hikoso[1], Osamu Yamaguchi[1], Manabu Taneike[1,2], Toshihiro Takeda[1], Takahito Tamai[1], Jota Oyabu[1], Tomokazu Murakawa[1], Hiroyuki Nakayama[3], Kazuhiko Nishida[1,2], Shizuo Akira[4,5], Akitsugu Yamamoto[6], Issei Komuro[1] & Kinya Otsu[1,2]

Heart failure is a leading cause of morbidity and mortality in industrialized countries. Although infection with microorganisms is not involved in the development of heart failure in most cases, inflammation has been implicated in the pathogenesis of heart failure[1]. However, the mechanisms responsible for initiating and integrating inflammatory responses within the heart remain poorly defined. Mitochondria are evolutionary endosymbionts derived from bacteria and contain DNA similar to bacterial DNA[2–4]. Mitochondria damaged by external haemodynamic stress are degraded by the autophagy/lysosome system in cardiomyocytes[5]. Here we show that mitochondrial DNA that escapes from autophagy cell-autonomously leads to Toll-like receptor (TLR) 9-mediated inflammatory responses in cardiomyocytes and is capable of inducing myocarditis and dilated cardiomyopathy. Cardiac-specific deletion of lysosomal deoxyribonuclease (DNase) II showed no cardiac phenotypes under baseline conditions, but increased mortality and caused severe myocarditis and dilated cardiomyopathy 10 days after treatment with pressure overload. Early in the pathogenesis, DNase II-deficient hearts showed infiltration of inflammatory cells and increased messenger RNA expression of inflammatory cytokines, with accumulation of mitochondrial DNA deposits in autolysosomes in the myocardium. Administration of inhibitory oligodeoxynucleotides against TLR9, which is known to be activated by bacterial DNA[6], or ablation of *Tlr9* attenuated the development of cardiomyopathy in DNase II-deficient mice. Furthermore, *Tlr9* ablation improved pressure overload-induced cardiac dysfunction and inflammation even in mice with wild-type *Dnase2a* alleles. These data provide new perspectives on the mechanism of genesis of chronic inflammation in failing hearts.

Mitochondrial DNA has similarities to bacterial DNA, which contains inflammatogenic unmethylated CpG motifs[2–4,7,8]. Damaged mitochondria are degraded by autophagy, which involves the sequestration of cytoplasmic contents in a double-membraned vacuole, the autophagosome and the fusion of the autophagosome with the lysosome[9]. Pressure overload induces the impairment of mitochondrial cristae morphology and functions in the heart[10,11]. We have previously reported that autophagy is an adaptive mechanism to protect the heart from haemodynamic stress[5].

DNase II, encoded by *Dnase2a*, is an acid DNase found in the lysosome[12]. DNase II in macrophages has an essential role in the degradation of the DNA of apoptotic cells after macrophages engulf them[13]. In the present study, we hypothesized that DNase II in cardiomyocytes digests mitochondrial DNA in the autophagy system to protect the heart from inflammation in response to haemodynamic stress.

First, we examined the alteration of DNase II activity in the heart in response to pressure overload. In wild-type mice, pressure overload by thoracic transverse aortic constriction (TAC) induced cardiac hypertrophy 1 week after TAC and heart failure 8–10 weeks after TAC[5]. DNase II activity was upregulated in hypertrophied hearts, but not in failing hearts (Supplementary Fig. 1a). Immunohistochemical analysis showed infiltration of $CD45^+$ leukocytes, including $CD68^+$ macrophages in failing hearts (Supplementary Fig. 1b). Then, we stained the heart sections with PicoGreen[14], anti-LAMP2a and anti-LC3 (ref. 15) antibodies, which was used for the detection of DNA, lysosomes and autophagosomes, respectively (Supplementary Figs 1c, d and 2a). We observed PicoGreen- and LAMP2a-positive deposits and PicoGreen- and LC3-positive deposits in failing hearts, but not in hypertrophied hearts, suggesting the accumulation of DNA in autolysosomes in failing hearts.

We crossed mice bearing a $Dnase2a^{flox}$ allele[13] with transgenic mice expressing *Cre* recombinase under the control of the α-myosin heavy chain promoter (α-MyHC)[16], to produce $Dnase2a^{flox/flox}$;α-MyHC-Cre^+ ($Dnase2a^{-/-}$) mice. We used $Dnase2a^{flox/flox}$;α-MyHC-Cre^- littermates ($Dnase2a^{+/+}$) as controls. The resulting $Dnase2a^{-/-}$ mice were born at the expected Mendelian frequency. In $Dnase2a^{-/-}$ mice, we observed a 90.1% reduction in the level of *Dnase2a* messenger RNA (mRNA) and a 95.1% decrease in DNase II activity in purified adult cardiomyocyte preparation (Supplementary Fig. 3a, b). Physiological parameters and basal cardiac function assessed by echocardiography showed no differences between $Dnase2a^{+/+}$ and $Dnase2a^{-/-}$ mice (Supplementary Table 1). These results indicate that DNase II does not appear to be required during normal embryonic development or for normal heart growth in the postnatal period.

To clarify the role of DNase II in cardiac remodelling, $Dnase2a^{-/-}$ mice were subjected to TAC. DNase II activity was upregulated in response to pressure overload in $Dnase2a^{+/+}$ hearts and was lower in sham- and TAC-operated $Dnase2a^{-/-}$ hearts than that in the corresponding controls (Supplementary Fig. 3c). Twenty-eight days after TAC, 57.1% of $Dnase2a^{-/-}$ mice had died, whereas 85.7% of $Dnase2a^{+/+}$ mice were still alive (Fig. 1a). The $Dnase2a^{-/-}$ hearts showed left ventricular dilatation and severe contractile dysfunction 10 days after TAC (Fig. 1b–d and Supplementary Table 2). The lung-to-body weight ratio, an index of lung congestion, was elevated in TAC-operated $Dnase2a^{-/-}$ mice (Fig. 1e). The increases in the heart-to-body weight ratio and cardiomyocyte cross-sectional area by TAC were larger in $Dnase2a^{-/-}$ mice than in $Dnase2a^{+/+}$ mice (Fig. 1e, f). TAC-operated $Dnase2a^{-/-}$ hearts showed massive cell infiltration (Fig. 1f). Immunohistochemical analysis of the hearts showed infiltration of $CD45^+$ leukocytes, including $CD68^+$ macrophages (Supplementary Fig. 4a). The mRNA level of interleukin (IL)-6 (*Il6*) was upregulated, but not other cytokine mRNAs in TAC-operated $Dnase2a^{-/-}$ hearts (Supplementary Fig. 4b). TAC-operated $Dnase2a^{-/-}$ hearts showed intermuscular and perivascular fibrosis with increased

[1]Department of Cardiovascular Medicine, Osaka University Graduate School of Medicine, Suita, Osaka 565-0871, Japan. [2]Cardiovascular Division, King's College London, London SE5 9NU, UK. [3]Department of Clinical Pharmacology and Pharmacogenomics, Graduate School of Pharmaceutical Sciences, Osaka University, Suita, Osaka 565-0871, Japan. [4]Laboratory of Host Defense, WPI Immunology Frontier Research Center, Osaka University, Suita, Osaka 565-0871, Japan. [5]Department of Host Defense, Research Institute for Microbial Diseases, Osaka University, Suita, Osaka 565-0871, Japan. [6]Faculty of Bioscience, Nagahama Institute of Bio-Science and Technology, Nagahama, Shiga 526-0829, Japan.

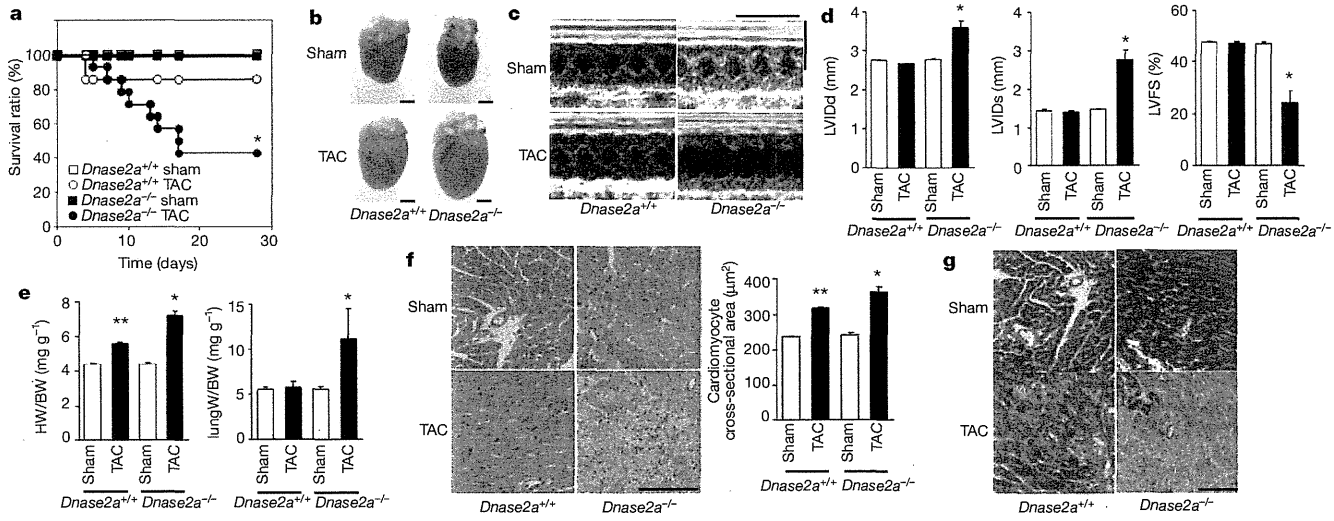

Figure 1 | TAC-induced cardiomyopathy in *Dnase2a*$^{-/-}$ mice. **a**, Survival ratio after TAC ($n = 7$–14 per group). **b**–**g**, Ten days after TAC. **b**, Gross appearance of hearts. Scale bar, 2 mm. **c**, Echocardiography. Scale bars, 0.2 s and 5 mm. Echocardiographic (**d**) and physiological (**e**) parameters ($n = 7$–13 per group). LVIDd and LVIDs, end-diastolic and end-systolic left ventricular internal dimension, respectively; LVFS, left venticular fractional shortening; HW/BW, heart/body weight. Haematoxylin and eosin-stained (**f**) and azocarmine and aniline blue (AZAN)-Mallory-stained (**g**) heart sections. Scale bar, 100 μm. Data are mean ± s.e.m. $^{*}P < 0.05$ versus all other groups, $^{**}P < 0.05$ versus sham-operated controls.

mRNA expression of α2 type I collagen (*Col1a2*) (Fig. 1g and Supplementary Fig. 3d). Ultrastructural analysis of TAC-operated *Dnase2a*$^{-/-}$ hearts showed a disorganized sarcomere structure, misalignment and aggregation of mitochondria, and aberrant electron-dense structures (Supplementary Fig. 4c). The mRNA levels of atrial natriuretic factor (*Nppa*) and brain natriuretic peptide (*Nppb*) were higher in TAC-operated *Dnase2a*$^{-/-}$ mice than in TAC-operated *Dnase2a*$^{+/+}$ mice (Supplementary Fig. 3d). These data suggest that DNase II plays an important role in preventing pressure overload-induced heart failure and myocarditis.

To clarify the molecular mechanisms underlying the cardiac abnormalities observed in *Dnase2a*$^{-/-}$ mice, we evaluated the phenotypes in the earlier time course after pressure overload. Chamber dilation and cardiac dysfunction developed with time after TAC in *Dnase2a*$^{-/-}$ mice (Supplementary Fig. 5a). We chose to perform the analysis 2 days after TAC to minimize the contributions of operation-related events and phenomena secondary to the initial and essential molecular event that induced cardiomyopathy. TAC-operated *Dnase2a*$^{-/-}$ hearts showed cell infiltration without apparent fibrosis (Fig. 2a, b) and infiltration of CD68^{+} macrophages and Ly6G^{+} cells (Fig. 2c). We detected increases in the mRNA levels of IL-1β (*Il1b*) and *Il6*, but not interferon-β (*Ifnb1*) and -γ (*Ifng*) or tumour-necrosis factor (TNF)-α in TAC-operated *Dnase2a*$^{-/-}$ hearts (Supplementary Fig. 6a). To identify the source of IL-1β and IL-6, we performed *in situ* hybridization analysis in heart sections. *Il1b* and *Il6* mRNA-positive cardiomyocytes were evident in TAC-operated *Dnase2a*$^{-/-}$ hearts (Supplementary Fig. 4d).

Ultrastructural analysis showed aberrant electron-dense deposits without apparent changes in sarcomeric and mitochondrial structures

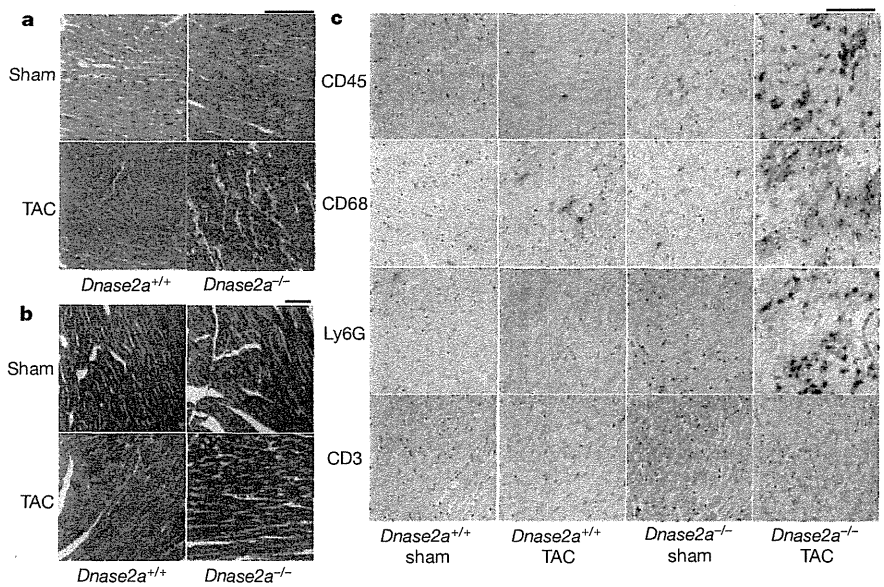

Figure 2 | Pressure overload-induced inflammatory responses in *Dnase2a*$^{-/-}$ mice 2 days after TAC. Mice were analysed 2 days after TAC (**a**–**c**). **a**, Haematoxylin and eosin-stained heart sections. Scale bar, 100 μm. **b**, AZAN-Mallory-stained sections. Scale bar, 100 μm. **c**, Immunohistochemical analysis using antibodies to CD45, CD68, Ly6G and CD3. Scale bar, 100 μm.

in TAC-operated *Dnase2a*$^{-/-}$ hearts (Fig. 3a). At higher magnification, the electron-dense deposits appeared to be autolysosomes (Fig. 3a). Immunoelectron microscopic analysis using anti-DNA antibody showed DNA deposition in autolysosomes (Fig. 3b). In TAC-operated *Dnase2a*$^{-/-}$ hearts, we observed PicoGreen- and LAMP2a-positive deposits and PicoGreen- and LC3-positive deposits (Supplementary Figs 2b and 6b, c). The PicoGreen-positive deposits were not TdT-mediated dUTP nick end labelling (TUNEL)-positive (Supplementary Fig. 6d), indicating that the DNA was not derived from fragmented nuclear DNA. To label mitochondrial DNA, mice were injected with 5-ethynyl-2′-deoxyuridine (EdU) five times before TAC. EdU, a nucleoside analogue to thymidine, is incorporated into DNA during active DNA synthesis[17]. EdU specifically binds to mitochondrial DNA during its active DNA synthesis in non-dividing cardiomyocytes. In TAC-operated *Dnase2a*$^{-/-}$ hearts, we observed EdU- and LAMP2a-positive deposits and EdU- and LC3-positive deposits (Fig. 3c, d and Supplementary Fig. 2c), indicating that mitochondrial DNA accumulated in autolysosomes.

The innate immune system is the major contributor to acute inflammation induced by microbial infection[18]. TLR9, localized in the endolysosome, senses DNA with unmethylated CpG motifs derived from bacteria and viruses. Mitochondrial DNA activates polymorphonuclear neutrophils through CpG/TLR9 interactions[19]. Immunohistochemical analysis indicated that TLR9 was co-localized with EdU-positive deposits (Fig. 3e). TLR9 is activated by synthetic oligodeoxynucleotides (ODN1668) that contains unmethylated CpG[6], but it is inhibited by inhibitory ligands, such as ODN2088 (ref. 20), in which 'GCGTT' in ODN1668 is replaced with 'GCGGG'. ODN1668 induced increases in *Il1b* and *Il6* mRNA levels in wild-type isolated adult cardiomyocytes (data not shown). We, then, examined the effect of ODN2088 on carbonyl cyanide *m*-chlorophenyl hydrazone (CCCP) or isoproterenol-induced cell death using isolated adult cardiomyocytes to eliminate the contribution of immune cells[5]. CCCP, a protonophore, induces dissipation of mitochondrial membrane potential. Isoproterenol caused a loss of mitochondrial membrane potential in wild-type cardiomyocytes, as indicated by loss of tetramethylrhodamine ethyl ester signal (Supplementary Fig. 7a). Incubation with CCCP or isoproterenol induced conversion of LC3-I to LC3-II, an essential step during autophagosome formation, and treatment with the lysosomal inhibitor bafilomycin A1 led to an even larger increase of LC3-II in CCCP- or isoproterenol-treated cells than in control cells, indicating that CCCP or isoproterenol accelerated autophagic flux (Supplementary Fig. 7b). Isolated cardiomyocytes from *Dnase2a*$^{-/-}$ hearts were more susceptible than those from control hearts to CCCP or isoproterenol in the presence of

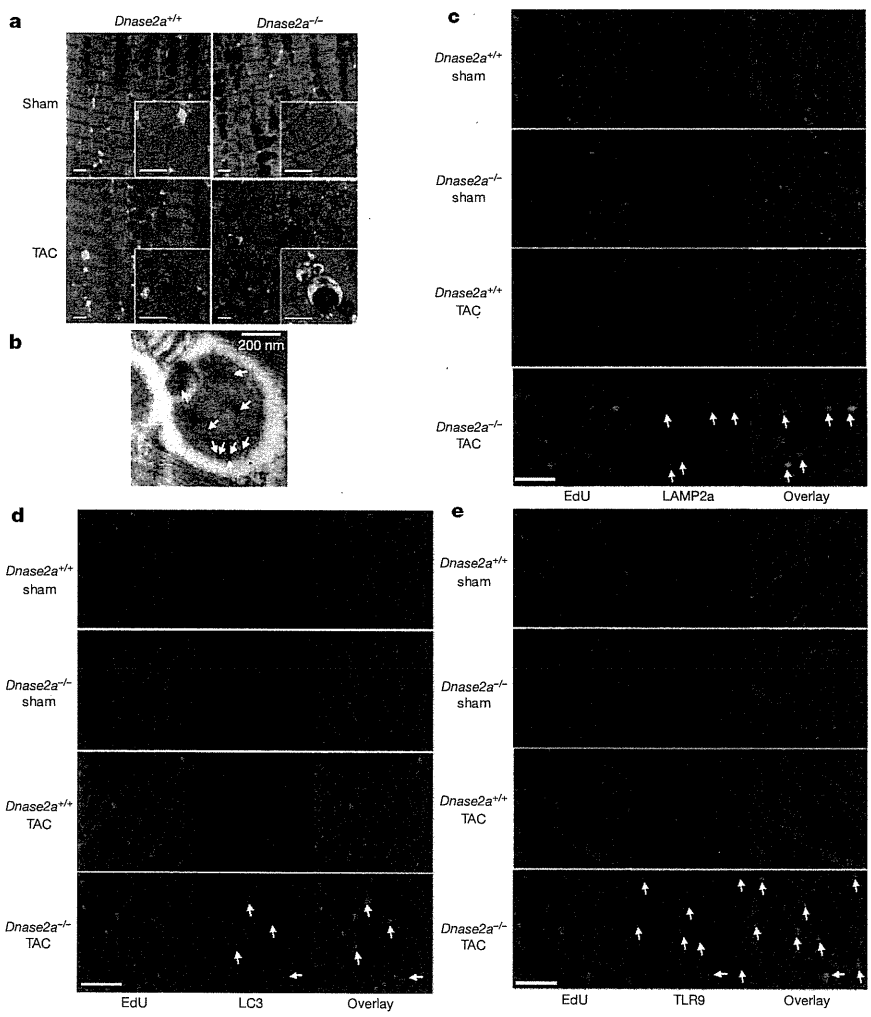

Figure 3 | Deposition of mitochondrial DNA in autolysosomes in pressure-overloaded *Dnase2a*$^{-/-}$ hearts. Mice were analysed 2 days after TAC (**a**–**e**). **a**, Electron microscopic analysis. Images of mitochondria at higher magnification are shown in subsets. Scale bar, 1 μm. **b**, Autolysosome after incubation with anti-DNA antibody and 10 nm gold staining. Scale bar, 200 nm. Arrows indicate labelled DNA. Double staining of heart sections with EdU (green) and anti-LAMP2a antibody (red) (**c**), EdU (green) and anti-LC3 antibody (red) (**d**) or EdU and anti-TLR9 antibody (red) (**e**). Arrows indicate EdU-positive and LAMP2a-, LC3- or TLR9-positive structures. Scale bar, 10 μm.

inactive control oligodeoxynucleotides (ODN2088 control) (Supplementary Fig. 7c–e). CCCP upregulated the mRNA expression levels of *Il1b* and *Il6* in *Dnase2a*$^{-/-}$ cardiomyocytes (Supplementary Fig. 7f). Incubation of *Dnase2a*$^{-/-}$ cardiomyocytes with ODN2088 attenuated the cell death and cytokine mRNA induction by CCCP treatment. Treatment of the *Dnase2a*$^{-/-}$ cardiomyocytes with 3-methyladenine, an autophagy inhibitor, and rapamycin, an autophagy inducer, inhibited and enhanced the induction of the cytokine mRNA by CCCP treatment, respectively (Supplementary Fig. 7g).

We next examined whether the inhibition of TLR9 can rescue the cardiac phenotypes in TAC-operated *Dnase2a*$^{-/-}$ mice. Administration of ODN2088 resulted in the improvement of survival 28 days after TAC (Fig. 4a). ODN2088 attenuated chamber dilation and cardiac dysfunction compared with the control oligodeoxynucleotides 4 days after TAC (Fig. 4b, c and Supplementary Fig. 8a). In addition, ODN2088 inhibited infiltration of CD68$^+$ macrophages and Ly6G$^+$ cells, fibrosis and upregulation of *Il6*, *Ifng*, *Nppa* and *Col1a2* mRNAs in TAC-operated *Dnase2a*$^{-/-}$ hearts (Fig. 4d and Supplementary Fig. 8b–e). ODN2088 prevented cardiac remodelling for a longer time (end-diastolic left ventricular internal dimension (LVIDd), in millimetres, 2.74 ± 0.03, 2.76 ± 0.03; end-systolic left ventricular internal dimension (LVIDs), in millimetres, 1.37 ± 0.03, 1.34 ± 0.05; left ventricular fractional shortening (LVFS) (%), 50.1 ± 0.7, 51.4 ± 1.5, before and 14 days after TAC, respectively, $n = 6$). Furthermore, ablation of *Tlr9* rescued the cardiac phenotypes in TAC-operated *Dnase2a*$^{-/-}$ mice (Supplementary Fig. 9).

To examine the significance of TLR9 signalling pathway in the genesis of heart failure, we subjected TLR9-deficient mice[6] to TAC. Ten weeks after TAC, TLR9-deficient mice showed smaller left ventricular dimensions, better cardiac function and less pulmonary congestion than in TAC-operated control mice (Fig. 4e, f and Supplementary Fig. 10a). The extent of fibrosis, the levels of *Nppa*, *Nppb* and *Col1a2* mRNA, infiltration of CD68$^+$ macrophages were attenuated in TLR9-deficient mice (Supplementary Fig. 10b–e). We detected no significant differences in the cytokine mRNA levels between TAC-operated groups (Supplementary Fig. 10f). Furthermore, ODN2088 improved survival of wild-type mice in a more severe TAC model (Supplementary Fig. 10g). These data indicate that the TLR9 signalling pathway is involved in inflammatory responses in failing hearts in response to pressure overload and plays an important role in the pathogenesis of heart failure.

In this study, we showed that mitochondrial DNA that escapes from autophagy-mediated degradation cell-autonomously leads to TLR9-mediated inflammatory responses in cardiomyocytes, myocarditis and dilated cardiomyopathy. Immune responses are initiated and perpetuated by endogenous molecules released from necrotic cells, in addition to pathogen-associated molecular patterns expressed in invading microorganisms[21]. Cellular disruption by trauma releases mitochondrial molecules, including DNA, into circulation to cause systemic inflammation[19]. Depletion of autophagic proteins promotes cytosolic translocation of mitochondrial DNA and caspase-1-dependent cytokines mediated by the NALP3 inflammasome in response to

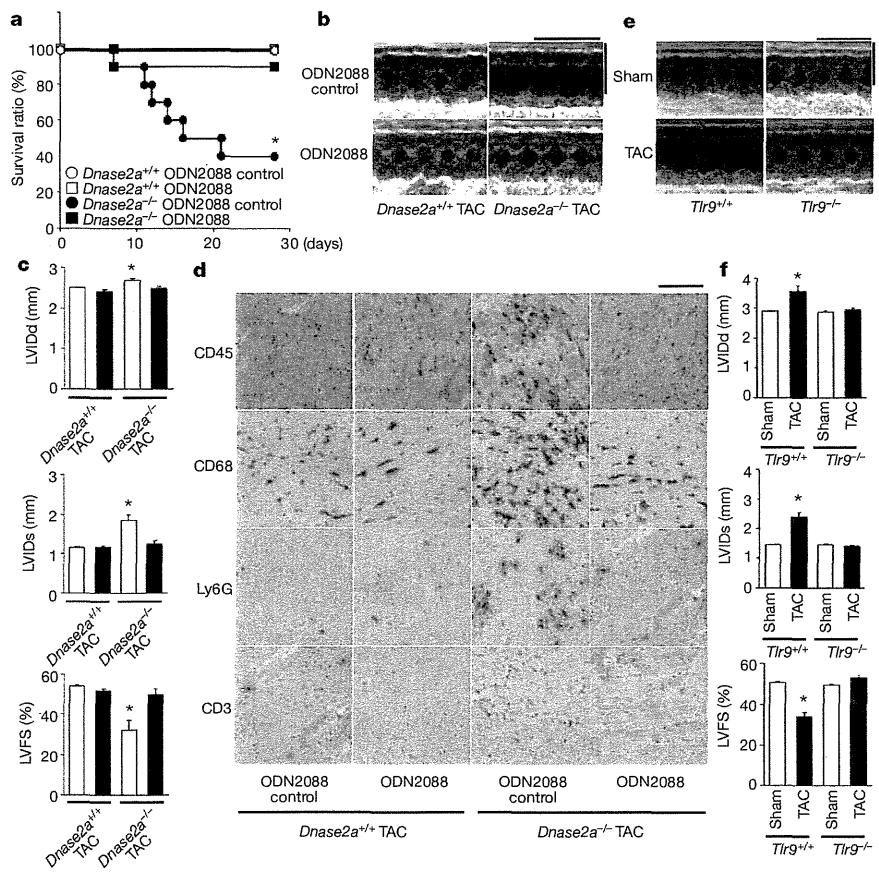

Figure 4 | Inhibition of TLR9 attenuated TAC-induced heart failure. **a**, Survival ratio of TAC-operated ODN-treated mice ($n = 6$–10 per group). **b–d**, Four days after TAC. **b**, Echocardiography. Scale bars, 0.2 s and 5 mm. **c**, Echocardiographic parameters. Open and closed bars represent ODN2088 control- and ODN2088-treated groups, respectively ($n = 5$–8 per group). **d**, Immunohistochemical analysis. Scale bar, 100 μm. TLR9-deficient mice were analysed 10 weeks after TAC (**e**, **f**). **e**, Scale bars, 0.2 s and 5 mm. **f**, Echocardiographic parameters ($n = 6$–10 per group). Data are mean ± s.e.m. *$P < 0.05$ versus all other groups.